THE ASTROPHYSICAL JOURNAL, 530:625–651, 2000 February 20

THE SURFACE BRIGHTNESS FLUCTUATION SURVEY OF GALAXY DISTANCES. II. LOCAL AND LARGE-SCALE FLOWS[1,2]

JOHN L. TONRY[3]
Institute for Astronomy, University of Hawaii, Honolulu, HI 96822; jt@ifa.hawaii.edu, jt@ifa.hawaii.edu
JOHN P. BLAKESLEE
Department of Astronomy, MS 105-24, California Institute of Technology, Pasadena, CA 91125; john@arneb.mit.edu
EDWARD A. AJHAR[3]
Kitt Peak National Observatory, National Optical Astronomy Observatories, P.O. Box 26732, Tucson, AZ 85726; ajhar@noao.edu
AND
ALAN DRESSLER
Carnegie Observatories, 813 Santa Barbara Street, Pasadena, CA 91101; dressler@omega.ociw.edu
Received 1999 July 2; accepted 1999 October 6

ABSTRACT

We present results from the Surface Brightness Fluctuation (SBF) Survey for the distances to 300 early-type galaxies, of which approximately half are ellipticals. A modest change in the zero point of the SBF relation, derived by using Cepheid distances to spirals with SBF measurements, yields a Hubble constant $H_0 = 77 \pm 4 \pm 7$ km s^{-1} Mpc^{-1}, somewhat larger than the *HST* Key Project result. We discuss how this difference arises from a different choice of zero point, a larger sample of galaxies, and a different model for large-scale flows. Our result is 4% larger than found in a recent comparison of the SBF Survey peculiar velocities with predictions derived from the galaxy density field measured by redshift surveys (Blakeslee et al. 1999b). The zero point of the SBF relation is the largest source of uncertainty, and our value for H_0 is subject to all the systematic uncertainties of the Key Project zero point, including a 5% decrease if a metallicity correction for the Cepheids is adopted. To analyze local and large-scale flows—departures from smooth Hubble flow—we use a parametric model for the distribution function of mean velocity and velocity dispersion at each point in space. These models include a uniform thermal velocity dispersion and spherical attractors whose position, amplitude, and radial shape are free to vary. Our modeling procedure performs a maximum likelihood fit of the model to the observations. Our models rule out a uniform Hubble flow as an acceptable fit to the data. Inclusion of two attractors, one of which having a best-fit location coincident with the Virgo cluster and the other having a fit location slightly beyond the Centaurus clusters (which we refer to by convention as the Great Attractor), reduces χ^2/N from 2.1 to 1.1. The fits to these attractors both have radial profiles such that $v \approx r^{-1}$ (i.e., isothermal) over a range of overdensity between about 10 and 1, but fall off more steeply at larger radius. The best-fit value for the small-scale, cosmic thermal velocity is 180 ± 14 km s^{-1}. The quality of the fit can be further improved by the addition of a quadrupole correction to the Hubble flow. The dipole velocity offset from the CMB frame for the volume we survey (amplitude $\sim$150 km s^{-1}) and the quadrupole may be genuine (though weak) manifestations of more distant density fluctuations, but we find evidence that they are more likely due to the inadequacy of spherical models to describe the density profile of the attractors. The residual dipole we find is comparable to the systematic error in these simple, parametrized models; in other words, our survey volume of $R < 3000$ km s^{-1} is, in a mass averaged sense, essentially at rest with respect to the CMB. This contradicts claims of large amplitude flows in much larger volumes that include our sample. Our best-fitting model, which uses attenuated power-law mass distributions for the two attractors, has enclosed mass overdensities at the Local Group of $7 \times 10^{14}\ M_\odot$ for the Virgo Attractor and $9 \times 10^{15}\ M_\odot$ for the Great Attractor. Without recourse to information about the overdensities of these attractors with respect to the cosmic mean we cannot provide a good constraint on Ω_M, but our data do give us accurate measurements in terms of δ, the overdensities of the enclosed masses with respect to the background: $\delta\ \Omega_M^{2/3} = 0.33$ for the Virgo Attractor and $\delta\ \Omega_M^{2/3} = 0.27$ for the Great Attractor.

Subject headings: distance scale — galaxies: clusters: individual (Virgo, Centaurus) — galaxies: distances and redshifts — large-scale structure of universe

[1] Observations in part from the Michigan-Dartmouth-MIT (MDM) Observatory.

[2] Based on observations with the NASA/ESA *Hubble Space Telescope*, obtained at the Space Telescope Science Institute, which is operated by the Association of Universities for Research in Astronomy (AURA), Inc., under NASA contract NAS 5-26555. These observations are associated with proposals ID 5910 and ID 6579.

[3] Guest observers at the Cerro Tololo Inter-American Observatory and the Kitt Peak National Observatory, National Optical Astronomy Observatories, which are operated by AURA, Inc., under cooperative agreement with the National Science Foundation.

1. INTRODUCTION

There is now convincing evidence that the evolution of large-scale structure is driven by intergalactic dark matter. Understanding the nature of this dark matter remains one of the major unsolved problems in astronomy. It is for this reason that mapping the overall mass distribution, independent of the distribution of luminous matter in galaxies, must be considered a fundamental endeavor in cosmological research. Unfortunately, few tools are available for the purpose: weak gravitational lensing can trace, statistically, the presence of intervening dark matter at large distances, and X-ray emitting gas can be used to map the gravitational potential of the dark matter that binds rich clusters. However, for a point-by-point comparison of the density of dark and luminous matter, measuring peculiar velocities—departures from pure Hubble flow caused by an uneven distribution of dark matter—is the only effective method available.

Using galaxies as test particles to sample the local gravitational field requires accurate knowledge of their positions in space, because galaxy motions are dominated by the expansion of the universe for all but the closest objects. Since most methods deliver an accuracy that (at best) scales proportionately with the distance, there is a premium on more accurate distance measurements driven by the desire to measure peculiar velocities over a large volume of space. The peculiar velocity that is known best, by far, is the 370 km s^{-1} motion of our Sun with respect to the cosmic microwave background (CMB), known with exquisite accuracy from the *COBE* measurement of the CMB dipole anisotropy, which is then converted with less certainty to the 627 km s^{-1} motion of our Local Group of galaxies with respect to the CMB. A study of peculiar velocities for other galaxies in the local universe can be thought of as an exercise with two complementary aims: (1) to map the dark matter distribution in the local universe and compare it with the local galaxy distribution (in the process, measuring a representative value of the cosmic density parameter Ω_M) and (2) to account for our Galaxy's motion as the consequence of anisotropies of the matter distribution. Such knowledge has application in interpreting large-scale structure inferred from the galaxy distribution alone, and in measuring the degree and nature of "bias" that may exist between the dark and luminous matter distributions, so important for testing theoretical models of structure formation. In addition, it is likely that a detailed comparison of the dark-matter/baryon/galaxy distributions on the scale of the correlation length for galaxies will shed light on the processes of galaxy formation and the role of dark matter in that process.

Large-scale deformations in the local Hubble flow in the form of a differential rotation of the Virgo Supercluster were first sought by Rubin (1951) and by de Vaucouleurs (1958). Later, considerations of the perturbations in the Hubble flow from the inhomogeneities inherent in gravitational instability led Silk (1974) and Peebles (1976) to predict and look for radial infall into the Virgo Supercluster. However, the claim by Rubin et al. (1976) of a bulk flow on the scale of 6000 km s^{-1} first galvanized extensive investigations into whether deformations in the Hubble flow were real. Unfortunately, the method of distance determination used in this pioneering work was too crude to fight its way through the Malmquist-like systematic errors that are endemic to the field. The first solid detections of large-scale flows and inferred dark structures began around 1980, including Tonry (1980), Schechter (1980), Yahil, Sandage, & Tammann (1980), Aaronson et al. (1980), Tonry & Davis (1981), and Aaronson et al. (1982a, 1982b), using spiral and elliptical galaxies to map the Local Supercluster. All studies detected the infall pattern that was anticipated for a sizeable overdensity roughly centered on the Virgo cluster, but with an amplitude at the position of the Local Group that ranged from 125 km s^{-1} (Yahil et al. 1980) to 480 km s^{-1} (Aaronson et al. 1980). As we shall see, the flow within the Virgo supercluster is much more complicated than these early models permitted, and this range of "infall velocity" is not surprising. One thing that was clear, however, was that in both amplitude and direction the pull of the Local Supercluster was insufficient to be the sole cause of the CMB dipole anisotropy, i.e., the motion of the Milky Way or Local Group with respect to the CMB. An additional pull, in the direction of the Centaurus supercluster, implicated as well by the high galaxy density in this direction, was suggested by Shaya (1984), Tammann & Sandage (1985), and Aaronson et al. (1986). Of particular relevance for the discussion of our own results is the suggestion by Lilje, Yahil, & Jones (1986) that the effect of this more distant mass can be seen as a quadrupole term in the peculiar velocity field of the Local Supercluster.

Based on a refined distance estimator for elliptical galaxies, actually a projection of the fundamental plane (Dressler et al. 1987; Djorgovski & Davis 1987), Lynden-Bell et al. (1988) used a sample of over 400 elliptical galaxies to map a much larger volume of space. This study confirmed the infall pattern toward Virgo but credited a considerable fraction of the peculiar velocity measured for local galaxies to the quadrupole of a more distant mass concentration. Surprisingly, however, the Lynden-Bell et al. study did not find the Centaurus cluster to be the center of a more distant infall pattern, but put the center at a distance approximately 50% greater, with Centaurus and its associated groups themselves falling into the more distant attractor at a velocity of order 1000 km s^{-1}. The pull on the Local Group from this "behind Centaurus" attractor was reckoned to be of order 500 km s^{-1}, perhaps twice as big as the Virgo pull but from a velocity distance of around 4000 km s^{-1}, over 3 times as distant. The implied order of magnitude greater mass earned it the nickname "Great Attractor" (GA).

However, doubts have remained about whether the GA is indeed a well-defined overdensity with such a large gravitational influence. While Dressler & Faber's (1990a, 1990b) distance measurements of additional elliptical and spiral galaxies appeared to show the distinctive S-shaped pattern of infall, including "backside infall," the larger spiral sample of Mathewson, Ford, & Buckhorn (1992) did not. Instead, these authors argued for a continuing high amplitude flow beyond the distance identified as the GA center, perhaps the result of a more distant gravitational pull, such as the "Giant Attractor" suggested by Scaramella et al. (1989) associated with the Shapley concentration of rich clusters, more than 3 times as distant as the GA.

Further evidence that the GA's role in producing the local flow pattern might have been overestimated is discussed by Courteau et al. (1993). Adding a more complete sample of spirals, particularly in the Perseus-Pisces region, led to this study's finding of a considerable amplitude "bulk

flow"—that is, a nonconverging flow whose source, if gravitational in origin, would be on a scale considerably larger than 6000 km s^{-1}, a region encompassing the GA. This lingering uncertainty in the sources of the local flow pattern—that is, the contribution of the Local Supercluster, the GA, Perseus-Pisces, the Shapley concentration, and structures beyond—have been made all the more important by studies of Lauer & Postman (1994), Willick (1999), and Hudson et al. (1999), who find large, but not always consistent bulk flows, over even larger volumes of the local universe. Indeed, these flows have amplitudes large enough, over such large volumes, that they appear inconsistent with the small-scale anisotropy $\Delta T/T \sim 10^{-5}$ measured for CMB fluctuations.

However, recent studies of spiral galaxy distances by Giovanelli et al. (1999) and Dale et al. (1999) contradict this result by claiming that all of the Local Group's motion with respect to the CMB can be accounted for by sources within the $V = 6000$ km s^{-1} sphere. Studies of the fundamental plane of cluster galaxies by Gibbons, Fruchter, & Bothun (1999) also find a small bulk flow with respect to the CMB, as do the Type Ia supernovae observations of Riess, Press, & Kirshner (1995) which suggest that the more distant frame is at rest with respect to the CMB. Preliminary results reported at the 1999 July meeting on "Cosmic Flows" in Victoria by Courteau et al. (1999) on the Shellflow project, and by Colless et al. (1999) on the EFAR survey also find a bulk flow in the CMB frame which is consistent with zero.

The surface brightness fluctuation (SBF) method (Tonry & Schneider 1988) of measuring early-type galaxy distances is perhaps the most promising means for understanding these issues and resolving the disagreements. A recent comprehensive review of the SBF method is given by Blakeslee, Ajhar, & Tonry (1999a). Tonry et al. (1997) show that SBF offers an accuracy several times greater than either Tully-Fisher or Fundamental Plane distances (~ 0.1 mag vs. ~ 0.4 mag); as a consequence, its susceptibility to Malmquist-like biases is reduced by an order of magnitude. SBF also includes an implicit correction for variations in age and metal abundance, in the form of color term, which previous methods for measuring distances to elliptical galaxies did not include. The data we present here will have bearing on all the issues raised above, but they are limited to relatively nearby galaxies ($v < 4000$ km s^{-1}) for all but a handful of observations with the *Hubble Space Telescope* (*HST*). Nevertheless, we expect that future observations will eventually produce a highly accurate map of the distribution of matter out to distances of 10,000 km s^{-1} or more.

In this paper we will discuss the characteristics of our SBF data set and use the data to construct parametric models of the local flow pattern. We will show not only that the convergent flows into the Local Supercluster and Great Attractor dominate the departures from smooth Hubble flow but also that the data are sufficiently accurate to provide other constraints on bulk flow, local voids, and other possible attractors. The combination of these two attractors and a moderate thermal component accounts for 90% of the variance in our sample. Specifically, evidence for the GA comes not only from the large peculiar velocities in the Centaurus direction but also from the clear quadrupole signature in the Local Supercluster flow, whose amplitude and direction are consistent with an order of magnitude larger mass concentration in the Centaurus direction. The amplitude and scale of these two flows are consistent with low-Ω_M cosmologies and with the measured small-scale anisotropy of the CMB.

We extensively explore the covariances between various model parameters, such as the attractor distances and amplitudes, the Hubble parameter, and the overall bulk flow. The uncertainties will greatly diminish when additional *HST* SBF measurements spanning the GA region are available. A future paper will discuss more detailed models for the GA and compare our results to previous works, including a point-by-point comparison of SBF and Lynden-Bell et al. distances. In addition, while we have chosen on this first examination of our data to use *only* the peculiar velocity information inherent in the SBF distances and to completely ignore the distribution of galaxies, we intend in future papers to compare the SBF peculiar velocities in detail with the galaxy density field. Blakeslee et al. (1999b) have taken a first step in this direction.

2. THE DATA

2.1. *The SBF Distance Survey*

The first paper of this series (Tonry et al. 1997, hereafter SBF-I) described the galaxy sample and observations of the SBF survey in detail and gave a new calibration of the method. That calibration was derived by comparing averaged SBF measurements within seven galaxy groups to Cepheid distances to spirals purportedly within the same groups. It gave an absolute magnitude $\overline{M}_I^0 = -1.74$ at our fiducial early-type galaxy color of $(V-I)_0 = 1.15$. The alternative, direct calibration from SBF measurements for five Cepheid-bearing galaxies gave a brighter zero point of $\overline{M}_I^0 = -1.82$. As these two zero points agreed within the uncertainty, and because of the potential for systematic differences arising from the relative difficulty of SBF measurements in spiral bulges, we felt more secure in adopting the group calibration.

For a number of reasons it has become necessary to revisit the calibration issue. First of all, we wish to incorporate all the latest *HST* Cepheid distances: we adopt the values from Ferrarese et al. (1999), who for purposes of homogeneity have made a number of small revisions to earlier published results. A bigger change is that we have switched to the extinctions of Schlegel, Finkbeiner, & Davis (1998, hereafter SFD), determined from the *COBE*/DIRBE and *IRAS*/ISSA dust maps. These have better spatial resolution, uniformity, and accuracy than the old estimates derived from H I maps (Burstein & Heiles 1984, hereafter BH).

While there is a good correlation between the SFD and BH reddening estimates, there is also a significant zero-point offset, with SFD finding a mean extinction greater by 0.02 mag in $E(B-V)$ than BH. Therefore, correcting the SBF magnitudes and colors according to SFD should in general result in a different numerical value for $\overline{M}_I^0$. In the ideal universe, this zero-point change would be perfectly compensated by corresponding changes in the estimated extinctions to individual survey galaxies. For instance, because of the sensitivity of $\overline{M}_I$ to $(V-I)$ color, increasing the extinction estimate to any given galaxy by $\delta E(B-V)$, *while keeping the zero point fixed*, causes the SBF distance modulus for the galaxy to *increase* by

$$\delta(m-M) = [4.5(A_V - A_I) - A_I] \times \delta E(B-V)\,, \quad (1)$$

where A_V and A_I are the ratios of the total V- and I-band extinctions to the selective $E(B-V)$ extinction. The average

change of $\sim +0.02$ mag in $\delta E(B-V)$ gives a mean $\delta(m-M) \sim +0.1$ mag, again *for a fixed zero point*. However, if all the calibrator galaxies undergo the same change in extinction, then the zero point we derive from the Cepheid comparison will also change by $\delta\overline{M}_I^0 \sim +0.1$ mag, and the overall distance scale will not change. Because of small number statistics and the imperfect correlation between BH and SFD extinctions, this is not quite the case. The group-derived calibration now gives $\overline{M}_I^0 = -1.61 \pm 0.03$, and the direct Cepheid-galaxy calibration gives $\overline{M}_I^0 = -1.74 \pm 0.08$, where we have adopted a median for the latter value (see Appendix B).

In contrast to the approach of SBF-I, we opt for the direct calibration over the group one. The new calibration, based on all the latest measurements and the SFD extinctions, used here is

$$\overline{M}_I = -1.74 + 4.5[(V-I)_0 - 1.15] \, . \qquad (2)$$

The decision to switch to the direct calibration was inspired by indications that the *HST* Cepheid-bearing spirals may be systematically in the foreground for Virgo and other groups (see Ferrarese et al. 1999). Kelson et al. (2000) use simulations to estimate that this effect is at the 0.1 mag level, consistent with the difference we find between the group and galaxy calibrations. Equation (2) is within 0.07 mag of the theoretical calibration from the stellar population models of Worthey (1994) (see discussions by SBF-I and Blakeslee et al. 1999a). It is slightly fainter than the Ferrarese et al. calibration for two reasons: they used the extinction ratios from Cardelli, Clayton, & Mathis (1989) whereas we have used the ones recommended by SFD, and we have used a median rather than an average. We emphasize that despite the numerical coincidence of our new calibration with SBF-I, the increase in average extinction (eq. [1]) means that our distance moduli increase on average by $\sim$0.1 mag. Appendix B provides complete details on our choice of zero point and a discussion of the uncertainties in the different calibrations.

Finally, the survey data reductions were not yet complete at the time of SBF-I. In particular, we have added a large body of new measurements from the 2.4 m Las Campanas telescope that were generally taken under superior conditions and have enabled us to improve some distances. From detailed comparisons of these new data to older, poorer quality data, we discovered that bad data sometimes yield spurious SBF signals. We have found two simple quantities useful in comparing data qualities: PD = PSF $\times$ $v_{\rm CMB}$, where PSF is the full width at half-maximum of the point spread function in arcseconds and $v_{\rm CMB}$ is the CMB velocity in units of 1000 km s^{-1}, and a "quality" $Q = \log_2 [N_e(\overline{m})/{\rm PD}^2]$, where $N_e(\overline{m})$ is the number of electrons that would be detected in the image from an object with fluctuation magnitude $\overline{m}$ (estimated from the absolute fluctuation magnitude $\overline{M} \sim -1.74$ and CMB velocity for distance in order to avoid circularity), and PD^2 is proportional to the metric area within a resolution element, hence the number of stars for fixed surface brightness. The quality, therefore, involves the ratio of the variance from photon statistics to the variance from star-counting statistics and is high when many photons are collected per star. When PD > 2.7 or $Q < 0$, the observation is marked as unreliable and ignored (see § 2.3). For multiple observations of a given galaxy, we adopt a weighted average if the difference in PD is less than 0.3 or if each individual observation has PD < 1.3; otherwise, we reject the observation with the larger PD.

The entire SBF Survey data set will be published in a forthcoming supplementary paper (Tonry et al. 2000, in preparation).

2.2. *HST Data*

We incorporate eight distances from *HST* SBF observations: four from Lauer et al. (1998), NGC 4373 from Pahre et al. (1999), and three from our Cycle 6 program (Dressler et al. 2000). We have adjusted these distances slightly from the published ones to agree with the SFD extinctions and have revised the zero point from Ajhar et al. (1997) to agree with our new I-band zero point. Although the results presented here do not change significantly when the *HST* data are included (e.g., H_0 changes from 78.4 ± 2.8 with the eight *HST* points to 81.1 ± 5.4 when they are left out), they do become more robust to covariances between, for example, H_0 and infall amplitudes.

2.3. *Biases and Uncertainties*

When we compare these *HST* distances with the difficult ground-based efforts beyond 3000 km s^{-1} or so, we find that there may be a bias in the ground-based data that correlates with PD. Typical ground-based data for more nearby galaxies agree well with *HST* measurements (Ajhar et al. 1997; see also the discussion by Blakeslee et al. 1999a). However, at PD = 3 we find that d_{g-b}/d_{HST} ranges between 1 and 0.8, but we do not have enough *HST* observations to be confident that this is the onset of a bias in the ground-based data. If it truly is a bias, we believe the source could have origins including unresolved dust and structure, unresolved color gradients, and instrumental effects, and we cannot predict reliably when it may be present. We therefore restrict ourselves to PD < 2.7. When we fit our models to subsets of the data with different PD cuts, we find no change in the parameters to within the errors for $2.0 <$ PD < 3.5, which gives us confidence that we are not affected by a distance-dependent bias.

As in SBF-I, we try to verify the accuracy of our error estimates by looking at the scatter within groups. Since we do not know the radial extent of groups, we ask how much cosmic scatter in $\overline{M}$ is necessary if the groups have no radial depth at all, and we find the answer is 0.10 mag. Conversely, if we assume that groups have the same depth as breadth then the SBF cosmic scatter is 0.06 mag. Including this 0.06 mag of cosmic scatter in $\overline{M}_I$, the quartiles of the distribution in error in SBF distance modulus are 0.17, 0.21, and 0.29 mag, so this is a fairly sensitive test that the SBF error estimates are accurate. (Note that these errors are dominated by the observational compromises inherent in doing such a large survey on relatively small telescopes; in almost all cases the distances could be significantly improved.)

Because the differential volume increases with distance, there will be more galaxies scattered down in distance by the errors than are scattered up. The level of this Malmquist-like bias in our sample is difficult to quantify. We have the usual problem of not knowing what the true distribution of galaxies is, and we may also be subject to possible biases and selection effects which depend on distance. We try to minimize these effects by tailoring our exposure times and seeing conditions to the distance of the galaxy we are observing. In addition, we are not actually sampling a population that increases rapidly with distance

(mostly we tend to be seeing early-type galaxy in groups). Nevertheless, if we calculate the $e^{3.5(\delta d/d)^2}$ correction (Lynden-Bell et al. 1988) for the median error, we get a bias factor of 1.038. Including this correction in the models described below does not change the results, and in fact it slightly increases the χ^2 values.

The level of bias due to the irreducible cosmic scatter in $\overline{M}_I$ is very small. We preferentially measure galaxies to be too close because of their cosmic scatter at the 0.3% level (assuming 0.06 mag of cosmic scatter). Moreover, unlike the case for other methods, such as the "forward" Tully-Fisher relation, D_n-σ/fundamental plane, or SN Ia, that use some of the same observables (magnitude, effective radius, surface brightness) for the distance measurement as were used in the selection, the cosmic scatter in the $\overline{M}_I$-$(V-I)$ relation is not known to correlate with any observables measuring galaxy size or luminosity. The bottom line is that we can safely ignore bias correction for cosmic scatter, and because the dubiously applicable Malmquist bias factor of ~ 1.04 yields no measurable improvement, we ignore it.

The galaxy velocities come from ZCAT (Huchra et al. 1992, version dated 1998 November 23) and are converted to the CMB frame according to Lineweaver et al. (1996), and to the Local Group frame as defined by Yahil, Tammann, & Sandage (1977). (A recent study by Courteau & van den Bergh 1999 finds almost exactly the same Local Group reference frame.)

There are 336 galaxies in our sample, which is reduced to 295 after applying the PD < 2.7 cut. We restrict another 10 of these from contributing to the model fits, three because we think the SBF distance may be in error despite passing the PD cut, and seven because their velocities are quite discordant with our model velocity distribution function. The former cases include a messy galaxy at fairly low Galactic latitude with marginal seeing (NGC 6305), and galaxies with extremely blue color where we do not believe our calibration is reliable (NGC 5253 and IC 4182). The latter cases include three galaxies in Cen 45 (NGC 4709, NGC 4616, and D45), NGC 1400 (the high-velocity companion of NGC 1407 in Eridanus), NGC 4150 (a Coma I galaxy with a very low velocity), and NGC 4578 and NGC 4419, which we think have just passed through Virgo at high speed and therefore have extremely unusual velocities for their location.

3. MODELS OF LARGE-SCALE FLOWS

3.1. *Overview*

In this paper we shall limit ourselves to a simple, parametric model for the velocity field of galaxies. In addition, we try to avoid *all* group information. The assignment of galaxies to groups has had a checkered history, and we prefer to deal with the virial velocities directly, rather than trying to average them away.

There are two methods commonly used for constructing a merit function for a peculiar velocity model $V(r)$. The first is to assemble

$$\chi^2 = \sum \frac{[v_{\rm obs} - V(r)]^2}{\epsilon_v^2}\,, \tag{3}$$

where $\epsilon_v^2 = \delta r^2 + \delta v^2 + \sigma_v^2$, and δr is the uncertainty in position expressed in units of km s^{-1}, δv is the (small) uncertainty in the measurement of velocity, and σ_v is an allowance for thermal or virial velocity dispersion (cf. Hudson et al. 1997). This tacitly assumes that the slope $dV(r)/dr = H = 1$ everywhere, otherwise it is not correct to use distance error δr in the denominator. This can be very problematic for a model which has a significant disturbance to the Hubble flow, for example, in the local supercluster. It is possible to "correct" δr by a spatially varying $H(r)$, but then this χ^2 is no longer maximum likelihood (unless it includes the often neglected $-2\ln\sigma$ term) and will tend to bias parameters in such a way as to maximize $H\delta r$. The other weakness of this approach is that it involves some arbitrariness of when objects should be grouped and what virial velocity σ_v should be allocated for them.

The second common method (e.g., Davis, Strauss, & Yahil 1991; Strauss et al. 1992; Shaya, Tully, & Pierce 1992) is to invert the velocity model and use the observed velocity to provide a model distance which can be compared with the observed distance. This has the advantage that it compares the distances and model directly, but it has the disadvantage that it cannot cleanly deal with virial velocities, necessitating grouping to the point that virial velocity is reduced to a negligible magnitude compared to the flow velocity and distance error. It also has the disadvantage that the inversion of $V(r)$ can be multiple valued and is necessarily multiple valued in the regions of space where a supercluster flow is most prominently seen. One is then forced to an arbitrary or probabilistic choice of which model distance to use.

What we have chosen to do is to accept the fact that there is a distribution function of galaxy velocity which varies from place to place, both in mean velocity (large-scale flow) and in dispersion. Our models consist of a velocity distribution function at each location, $P(v\,|\,r)$, which we take to be Gaussian of mean $v_0(r)$ and dispersion $\sigma_v(r)$. A given distance measurement, itself a probability distribution, is multiplied by this model distribution function and integrated over distance, giving a velocity probability distribution. The merit function is then the likelihood, the product of these velocity distributions evaluated at the observed velocities.

The components of our model for the mean velocity $v_0(r)$ include a Hubble flow of amplitude H_0, a constant dipole velocity $\boldsymbol{w}$, possibly a quadrupole Q with zero trace which acts like an anisotropic Hubble constant, a density parameter Ω_M for the universe, and attractors which are assumed to be spherical power laws in density with a core and cutoff radius. The positions of these attractors can be free parameters as well as the power-law exponent, the core and cutoff radii, and the overall normalization. Our model for the velocity dispersion as a function of position, $\sigma_v(r)$, consists of the quadrature sum of an overall thermal velocity, a virial component at the center of each attractor, and possibly other (nonattracting) virial components at the locations of groups such as the Fornax cluster. These components have a velocity dispersion which varies spatially as $\exp(-r^2/2r_{\rm virial}^2)$. In principle we have enough distance accuracy to constrain both the background thermal component and these virial components (except for GA/Centaurus at the limit of our survey) with a smoothing length of perhaps 4 Mpc. In practice we fit only for the thermal background and Virgo velocity dispersions and put in by hand the Fornax (235 km s^{-1}) and Centaurus (500 km s^{-1}) dispersions with $r_{\rm virial} = 2$ Mpc. Unless otherwise stated, we use a thermal velocity dispersion of 187 km s^{-1}, which is the best-fit value in our most refined models.

Figure 1 illustrates how this works. The model $P(v \mid r)$ is shown along a line of sight near the Virgo cluster. The mean velocity has a Hubble flow term modified by a peculiar velocity which grows approximately as r^{-1} (for an r^{-2} density distribution) but then rolls off to zero at the center of the cluster because of the core radius in the density distribution. The velocity dispersion at each location consists of the quadrature sum of the thermal background component and a cluster velocity dispersion with an amplitude of about 650 km s^{-1}, which declines away from the Virgo cluster as a Gaussian of width 2 Mpc. Again, these parameters are all variable components of the velocity model.

This methodology deals cleanly with the "triple-valued zone" where the inversion of $V(r)$ is multiple valued. For example, along the line of sight in Figure 1, a velocity of 1400 km s^{-1} can occur at distances of 12, 17, and 22 Mpc, if there were no thermal or virial velocities. Our likelihood contribution will be large for distance measures which are close to any of those values since the inferred $P(v)$ will peak near 1400 km s^{-1}, and small at other distances (for models with small virial velocities). The real strength of this approach, however, is that it properly merges the effects of large-scale flows with the velocity dispersion.

With three shape parameters (power-law slope and core and cutoff radii), our attractor models have a lot of radial flexibility. The models can emulate anything from a centrally concentrated mass to an extended distribution with divergent total mass.

The question of spherical symmetry is harder to justify. We note, however, that the galaxy distribution in the Virgo supercluster is not completely flat, that the potential is much rounder than a mass distribution, and that the large-scale flows we see today arise from the time integral of the potential so that a spherical model might represent the velocity data quite well even though the potential is today significantly flattened. The question of how well a nonlinear spherical model matches N-body simulations was studied by Lee, Hoffman, & Ftaclas (1986), who concluded that in the mean it was not a bad approximation. Moreover, we do allow for the possibility of a quadrupole correction to the flow model, and this can start to modify a spherical flow into a more flattened one. As we shall see, there are indications that the Virgo Attractor is not spherical.

We convert a mass distribution to a peculiar velocity distribution using the usual nonlinear "nested Friedmann universe" model (e.g., Silk 1974), where each mass shell evolves from the Big Bang according to its interior mass density. We do not do this computation exactly, however, but rather use the Yahil (1985) "$\rho^{1/4}$ law" approximation

$$u_{\rm infall} = \tfrac{1}{3} H_0 r \Omega_M^{0.6} \delta (1+\delta)^{-1/4} , \qquad (4)$$

where r is the radius of the shell and δ is the mean mass density interior to the shell in units of the background density. Giavalisco et al. (1993) examined this approximation with N-body simulations and found that it is remarkably accurate for $-0.5 < \delta < 20$, which is the range of interest here. We do not expect our models to be valid all the way into the virialized core of the attractor ($\delta > 200$), so our velocity distribution function rolls over to zero in the mean at the centers of the attractors with a compensating rise in virial velocity dispersion.

It is common to recast this parametrization in terms of a local overdensity and peculiar velocity, which then permits Ω_M to be derived from this formula. However, because of our desire to avoid use of the galaxy distribution, we lack any a priori information about δ and thus have very little constraint on Ω_M. Only the nonlinear part of equation (4) provides any constraint at all, and clearly that is not going to be very reliable. Instead, we choose a single value for Ω_M and derive the overdensities for the model attractors from the fitted infall velocities.

3.2. *Details of Models*

The input to our models includes for each galaxy the position on the sky, distance and error, and velocity. The fitting program reads these data and also accepts a variety of model components, including cosmology (H_0, Ω_M, and dipole velocity $\boldsymbol{w}$), quadrupole (five components plus origin and cutoff), extended attractors, thermal components, and compact attractors. The program computes a model velocity distribution function for each observed data point, evaluates the probability of the observed velocity given the velocity probability distribution, forms the likelihood sum from the probabilities P—$\mathscr{L} = \sum \ln P$ + constant—and searches parameter space for a maximum in $\mathscr{L}$.

The model velocity field consists of a mean velocity at each point and associated Gaussian velocity dispersion. The Hubble constant and dipole velocity give a contribution to the model velocity $\boldsymbol{v}_{\rm model}$ at $\boldsymbol{r}$ of $\boldsymbol{w} + H_0 \boldsymbol{r}$. The quadrupole contributes a velocity at (x, y, z) of

$$e^{-r2/2r_{\rm quad}^2} \begin{pmatrix} Q_{xx} & Q_{xy} & Q_{xz} \\ Q_{xy} & Q_{yy} & Q_{yz} \\ Q_{xz} & Q_{yz} & Q_{zz} \end{pmatrix} \begin{pmatrix} x - x_Q \\ y - y_Q \\ z - z_Q \end{pmatrix} . \qquad (5)$$

The quadrupole matrix is forced to zero trace by insisting that $Q_{yy} = -Q_{xx} - Q_{zz}$, which ensures that the monopole H_0 parameter carries the net Hubble expansion proportional to distance. Unless otherwise specified, the origin of the quadrupole, $\boldsymbol{r}_Q$, is taken to be the Local Group, and the cutoff radius, $r_{\rm quad}$ is taken to be 50 Mpc, so that the Hubble flow becomes isotropic at large distance.

Extended attractors are modeled by starting with spherical density distributions of the form

$$\rho(r) = \frac{\rho_0}{(1 + r^3/r_c^3)^{\gamma/3}} , \qquad (6)$$

where γ is the power-law exponent and r_c is a core radius. This integrates nicely to give an enclosed mass function to which we append an exponential cutoff and divide by volume to get a mean enclosed overdensity:

$$\overline{\rho}(r) = \frac{\rho_0 \, e^{-r/r_{\rm cut}}}{1 - \gamma/3} \left(\frac{r}{r_c}\right)^{-3} \left[\left(1 + \frac{r^3}{r_c^3}\right)^{1-\gamma/3} - 1 \right] . \qquad (7)$$

After division by the background density, this can be plugged into equation (4) to calculate an infall velocity. Since the central density is finite, the flow velocity rolls over at approximately $r \approx r_c$ and approaches zero as $r \to 0$. We ordinarily normalize these attractors in terms of a velocity amplitude at our location by using the inverse of Yahil's $\rho^{1/4}$ law to convert such a velocity into an expression for ρ_0. The cutoff radius $r_{\rm cut}$ which appears in the exponential cutoff of the enclosed mass (mean overdensity in eq. [7]) ensures that these models have zero net mass and hence do not bias H_0 high by making a net local modification to Ω_M. For typical values of γ, $r_{\rm cut}$ is approximately where the density becomes negative and $\overline{\rho}(r)$ starts to decrease back to zero.

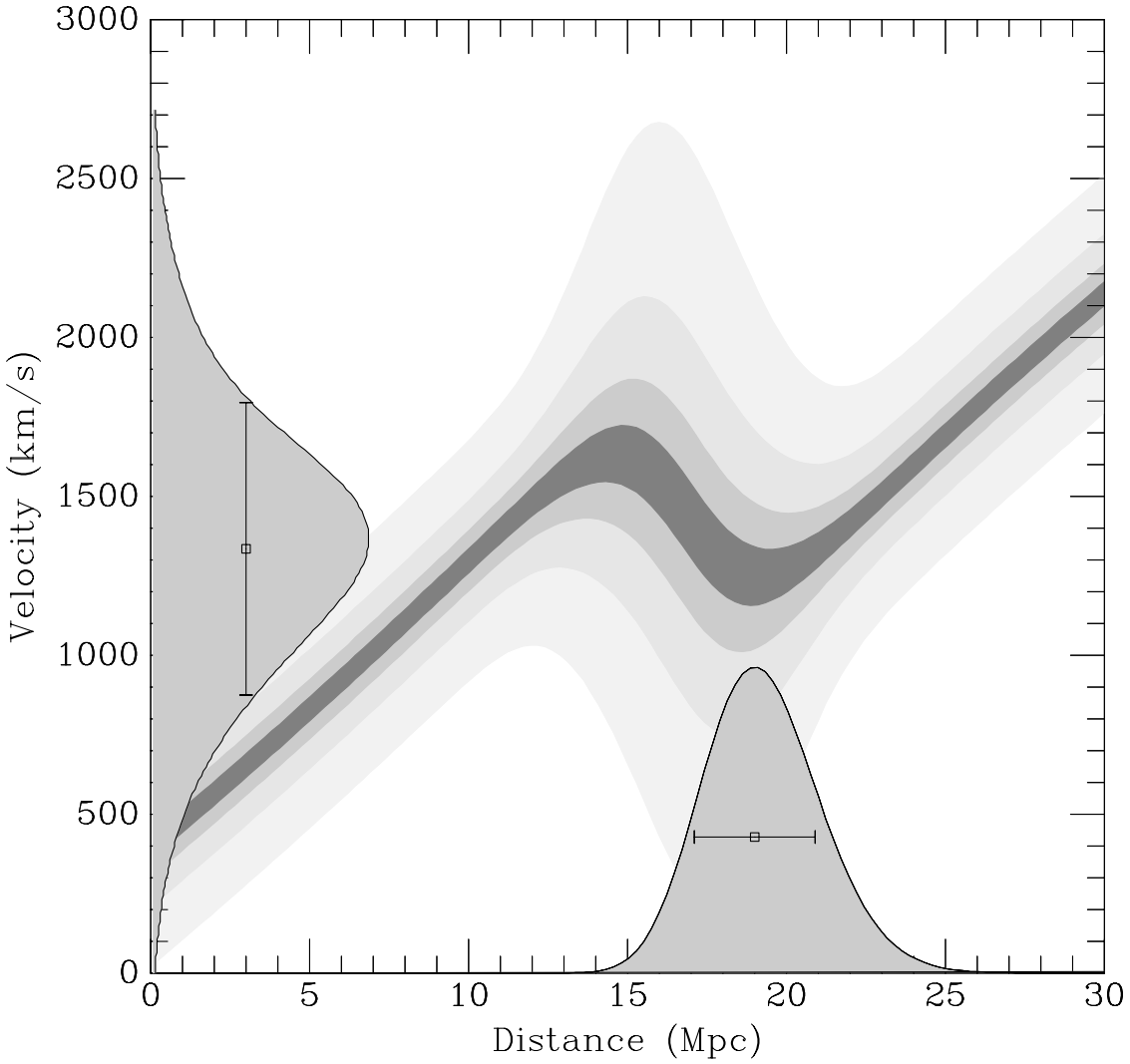

FIG. 1.—Model velocity distribution function $P(v \mid r)$ is shown for a line of sight which passes through the Virgo cluster. The different grayscale levels show the 2, 1, 0.5, and 0.2 σ points on the velocity distribution at a given distance. A distance observation is shown on the abscissa as a distance probability function, and the resulting velocity probability function is shown on the ordinate. This is evaluated at the observed velocity and forms a term in the likelihood product.

The covariance between the parameters γ, r_c, and $r_{\rm cut}$ makes it difficult to interpret values for any one parameter in isolation. We will strive to indicate what is well constrained by the models (e.g., mass of attractor, or run of peculiar velocity with radius) and what is not.

As mentioned above, the model velocity dispersion consists of the quadrature sums of background and extended thermal components. Each component has a velocity dispersion with a central value that falls off spatially according to a Gaussian of width $r_{\rm virial}$. These thermal components can either be specified explicitly (the cosmic dispersion is taken to be centered on the origin with an infinite Gaussian radius; Fornax is centered on the location of the Fornax cluster and has a core radius of 2 Mpc) or as part of an extended attractor. The thermal component of an extended attractor is centered on the attractor, has a parameter describing its central virial velocity dispersion, and shares the core parameter $r_{\rm virial}$ with the core radius r_c of the mean infall. (We expect $r_{\rm virial}$ to be close to r_c, and in our models we set the two radii to be the same.)

It is also possible to specify "Compact Attractors," density distributions which are Gaussians. These carry five parameters, their location, their Gaussian radius, and their amplitude. The amplitude is given in terms of the total mass and a fiducial radius, $R_{\rm fid} \equiv 50$ Mpc:

$$v_{\rm amp} = \frac{GM_{\rm tot}}{R_{\rm fid}^2} \frac{1}{H_0} \,. \tag{8}$$

For a Gaussian with $\rho = \rho_0 \exp(-r^2/2\tau^2)$, the enclosed mass is

$$M(r) = 4\pi\rho_0 \left[\sqrt{\frac{\pi}{2}}\, \tau^3 \, \mathrm{erf}\left(\frac{r}{\sqrt{2}\tau}\right) - \tau^2 r \exp\left(-\frac{r^2}{2\tau^2}\right)\right], \tag{9}$$

and $M_{\rm tot} = 4\pi\rho_0(\pi/2)^{1/2}\tau^3$. The expression for $M(r)$ is converted to a δ and then used in equation (4). The velocity amplitude can be made negative, which corresponds to a negative density void. Of course, the void cannot become deeper than the mean cosmological density. These compact attractors do not carry a thermal component.

We make no attempt to create an overall self-consistent density and velocity distribution—these components do not

interact with one another. Having specified the various components, the mean velocity is just the sum of the contributions of all the components, and the velocity dispersion is the quadrature sum of the various contributors.

Once we have a model, we then go about evaluating how well it matches our observations. For Gaussian statistics, we would have that the probability for making an observation v_i at a location r_i where our model predicts a mean velocity $V(r_i)$ and Gaussian dispersion $\sigma_v(r_i)$ is

$$P_i = \frac{1}{\sqrt{2\pi}\sigma_v(r_i)} \exp\left\{-\frac{1}{2}\left[\frac{v_i - V(r_i)}{\sigma_v(r_i)}\right]^2\right\}\Delta v \ . \quad (10)$$

The choice of Δv is arbitrary but represents how closely the model adheres to observation. We define the likelihood $\mathscr{L} = \ln \prod P_i$

$$\mathscr{L} = -\frac{1}{2}\sum\left[\frac{v_i - V(r_i)}{\sigma_v(r_i)}\right]^2 + \sum -\ln\sqrt{2\pi}\sigma_v(r_i) + \ln \Delta v \ . \quad (11)$$

The first term in $-2\mathscr{L}$ is just the usual definition of χ^2, and we can evaluate the goodness of fit according to the χ^2 per degree of freedom. If the dispersions $\sigma_v(r_i)$ do not depend on the parameters, then the second two terms can be ignored, since they are constant for a given set of observations and do not affect the choice of parameters which maximizes the joint probability.

Our situation is not quite so simple, because we believe we have errors which are normally distributed in log distance, and although our model distribution function has a Gaussian distribution of velocity at any point, the mean velocity and velocity dispersion vary as a function of position and hence are not a constant over the range where a given galaxy might lie. We deal with this for a galaxy of observed modulus $\mu \pm d\mu$ by forming a distance probability distribution that consists of 11 points between $\mu - 2\,d\mu$ to $\mu + 2\,d\mu$ weighted according to Gaussian statistics. The model is evaluated at each of these 11 points, providing a Gaussian velocity distribution with some mean and dispersion at each point. We sum these 11 Gaussians in velocity, weighted by their distance probabilities, to form a net probability distribution for the velocity we expect to see for this galaxy.

Our likelihood function is then simply formed by evaluating this probability at the observed velocity and summing a negative, normalized likelihood

$$\mathscr{N} = -2\sum\left[\ln P_i(v_i) + \ln(300\sqrt{2\pi})\right] , \quad (12)$$

where the constant term is introduced for Δv in order to shift the zero point of $\mathscr{N}$ into approximate agreement with χ^2. Deviations of $\mathscr{N}$ about its minimum, $\mathscr{N} - \mathscr{N}_{\rm min} = 2(\mathscr{L}_{\rm max} - \mathscr{L})$ are described approximately by a χ^2 distribution, so we use $\mathscr{N}$ to evaluate goodness of fit and confidence intervals on parameters. We also calculate a variance for the velocity distribution function we derive for each galaxy and use them to form a traditional χ^2. This χ^2 is useful for evaluating a goodness of fit but does *not* correspond to maximum likelihood and is not minimized for the best-fitting model.

4. FITS OF MODEL TO DATA

The model described in the previous section carries many parameters (five cosmological parameters, eight per attractor, five for a quadrupole, and four per thermal component), and there can be significant covariance between them, for example, γ and $r_{\rm cut}$, or w_x and $u_{\rm GA}$. We will first present a sequence of models which motivate our choices of mass components, starting with a Hubble flow and ending with two attractors contributing peculiar velocities.

We will subsequently look more carefully at these covariances and try to show what is well constrained by our data and what is not. For example, we cannot independently choose a unique γ and $r_{\rm cut}$, but all our models give nearly the same run of peculiar velocity between 6 and 20 Mpc from the center of the Virgo cluster. Distances will often be given in terms of their SGX, SGY, and SGZ components in the supergalactic coordinate system, defined in the RC3 (de Vaucouleurs et al. 1991).

It is extremely important not to force the models to conform to any particular velocity reference frame. For example, insisting on the CMB frame and using an r^{-2} density model for the Great Attractor leads to a very large infall velocity because of its covariance with w_x. We use the CMB frame for velocity data, but we always fit for an arbitrary dipole vector $\boldsymbol{w}$ as part of our models.

4.1. *A First Look*

Figure 2 shows all of the galaxies for which we have SBF distances plotted in a Hubble diagram—redshift in the CMB frame as a function of distance. The expansion of the universe is apparent, and a naive linear fit, without regard for error bars or the fact that the abscissa carries greater errors, yields a Hubble ratio of 73 km s^{-1} Mpc^{-1}. Figure 3 focuses on the more distant galaxies with smaller errors and plots Hubble ratio as a function of distance. Local peculiar velocities cause scatter in the Hubble ratio at distances of 40 Mpc, but it seems to settle down fairly well to an asymptotic value of 73 km s^{-1} Mpc^{-1}. However, as is seen in Figure 2, there is a lot of scatter in the Hubble plot, more than can be explained by distance error.

The near field Hubble flow is shown in Figure 4 in two different directions. Velocities in the Local Group frame are used to avoid the constant velocity offset incurred by using the CMB frame locally. It is possible to discern the important features of the local large-scale flow. The Virgo cluster

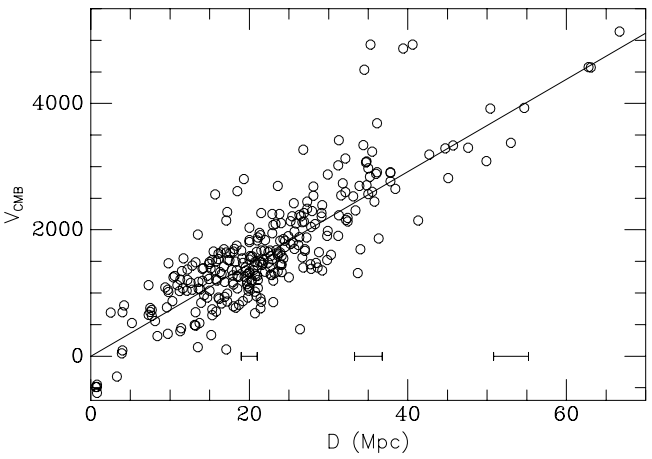

FIG. 2.—Recession velocities in the CMB frame are plotted as a function of distance. The line has a slope of 73 km s^{-1} Mpc^{-1}; the very deviant high points near 40 Mpc are Cen 45 galaxies. Typical 1 σ error bars are indicated; the most distant points are from *HST* and are relatively more accurate than nearby ones.

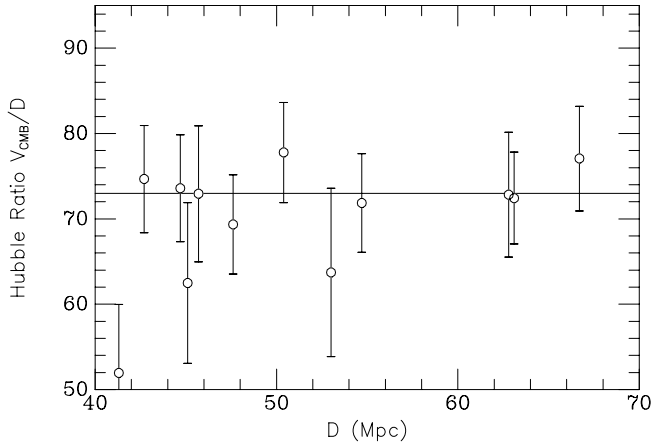

FIG. 3.—Hubble ratios (in CMB frame) are plotted as a function of distance for those points with small enough errors that the error in the Hubble ratio is less than 10 km s^{-1} Mpc^{-1}.

in the lower pane at SGY = +20 Mpc lies several hundred km s^{-1} below the Hubble flow—this is often referred to as our "infall velocity" toward Virgo. However, this is not the entire story, since the Fornax cluster at −20 Mpc *also* has a smaller velocity than the Hubble flow, but the quadrupole from a pure Virgo infall should cause it to have a larger velocity (although it is quite near the quadrupole null at 45°). Likewise, the quadrupole from a pure flow toward Virgo should cause the Hubble ratio to be smaller in a direction perpendicular to Virgo, but in fact we find a ratio in the upper panel which is slightly *larger* than the nominal Hubble flow. What we are seeing in these local galaxies are the effects of two flows, one toward Virgo and the other toward Centaurus in the −SGX direction.

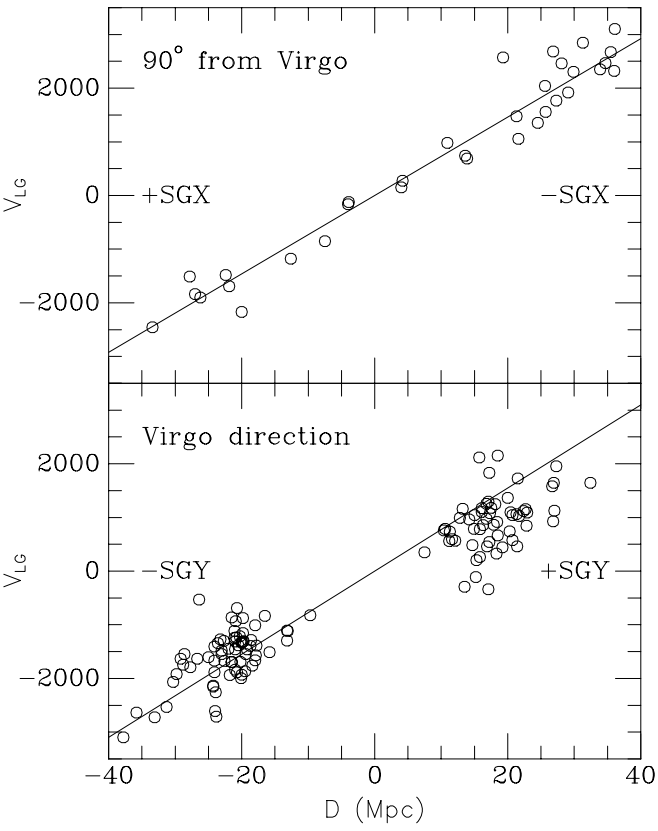

FIG. 4.—Recession velocities (in Local Group frame) are plotted as a function of distance in two directions. The upper panel shows galaxies which lie approximately in a 30° (half-angle) cone in the ±SGX direction, 90° away from the direction of Virgo. The lower panel shows galaxies which lie within a 15° cone toward Virgo (+SGY) and a 45° cone away from Virgo (which includes the Fornax cluster). A Hubble ratio of 73 km s^{-1} Mpc^{-1} is also drawn.

4.2. H_0 *Only*

We start by fitting the distances and velocities using a model which includes H_0 and a peculiar velocity $\boldsymbol{w}$, for a total of four free parameters. The sample consists of 285 galaxies. Allowing 187 km s^{-1} of thermal velocity but no additional virial velocities, we find $H_0 = 70$ km s^{-1} Mpc^{-1} and an overall dipole peculiar velocity of $\boldsymbol{w} = (-330, +180, -80)$ km s^{-1} in the CMB frame. The $\mathcal{N}$ for this model is 513, and χ^2 per degree of freedom (DOF, number of galaxies minus the number of parameters) for this model is $\chi^2_N = 2.08$. Note that $\mathcal{N}$ is not the same as χ^2: the former has an arbitrary offset defined in equation (12), and the latter is based on the difference between the observed and mean model velocity divided by the "velocity error bar" which is the variance of the probability distribution $P(v)$ calculated for each galaxy.

An obvious shortcoming of this model is that there is no allowance for virial velocities other than 187 km s^{-1} of background thermal velocity. If we add in additional thermal components for Fornax and Centaurus (235 and 500 km s^{-1}, which will be used throughout) and Virgo (650 km s^{-1}, which is about what we find when we fit for it), $\mathcal{N}$ drops considerably to $\mathcal{N} = 387$ and $\chi^2_N = 1.41$. In the CMB frame we again get $H_0 = 71$ with a negligibly different peculiar velocity of $\boldsymbol{w} = (-330, +200, -90)$.

Figure 5 illustrates residuals of velocities after removal of this model in the CMB frame. In all these vector field plots, the black points (falling stones) are blueshifted residuals which are greater than 1 σ, the white points (rising balloons) are redshifted residuals greater than 1 σ, and the gray points are residuals which are less than 1 σ in absolute value. The arrows indicate the magnitude of the residual according to the Hubble flow, i.e., an arrow of length 5 Mpc represents a velocity residual of 5 Mpc H_0 km s^{-1}. All the points are projected onto the supergalactic x-y plane, and the region where the galactic plane cuts through is darker gray. When galaxies are members of a group we plot only the group residual, so as to prevent the plot from becoming too overcrowded. The main failing of this model is obvious. The residuals near (−3, +16) are the Virgo "s-wave," positive peculiar velocities on the near side and negative on the far side of Virgo.

Another way of looking at the quality of the fit is to plot observed peculiar velocity as a function of model peculiar velocity. In order not to be overwhelmed by galaxies which have a large virial velocity (which does not appear in the mean model velocity), we plot only those galaxies where the model velocity uncertainty is less than 250 km s^{-1}. There appears to be a correlation in Figure 6 between model and observed, but the agreement is not good.

4.3. *Virgo Attractor Infall*

Adding an extended "Virgo Attractor" (VA) with $\gamma = 2$ near the location of the Virgo cluster at (−3.1, 16.6, −1.6) Mpc, we find an infall velocity at the Local Group of $u_{VA} = 101$ km s^{-1}, a Virgo thermal velocity dispersion of

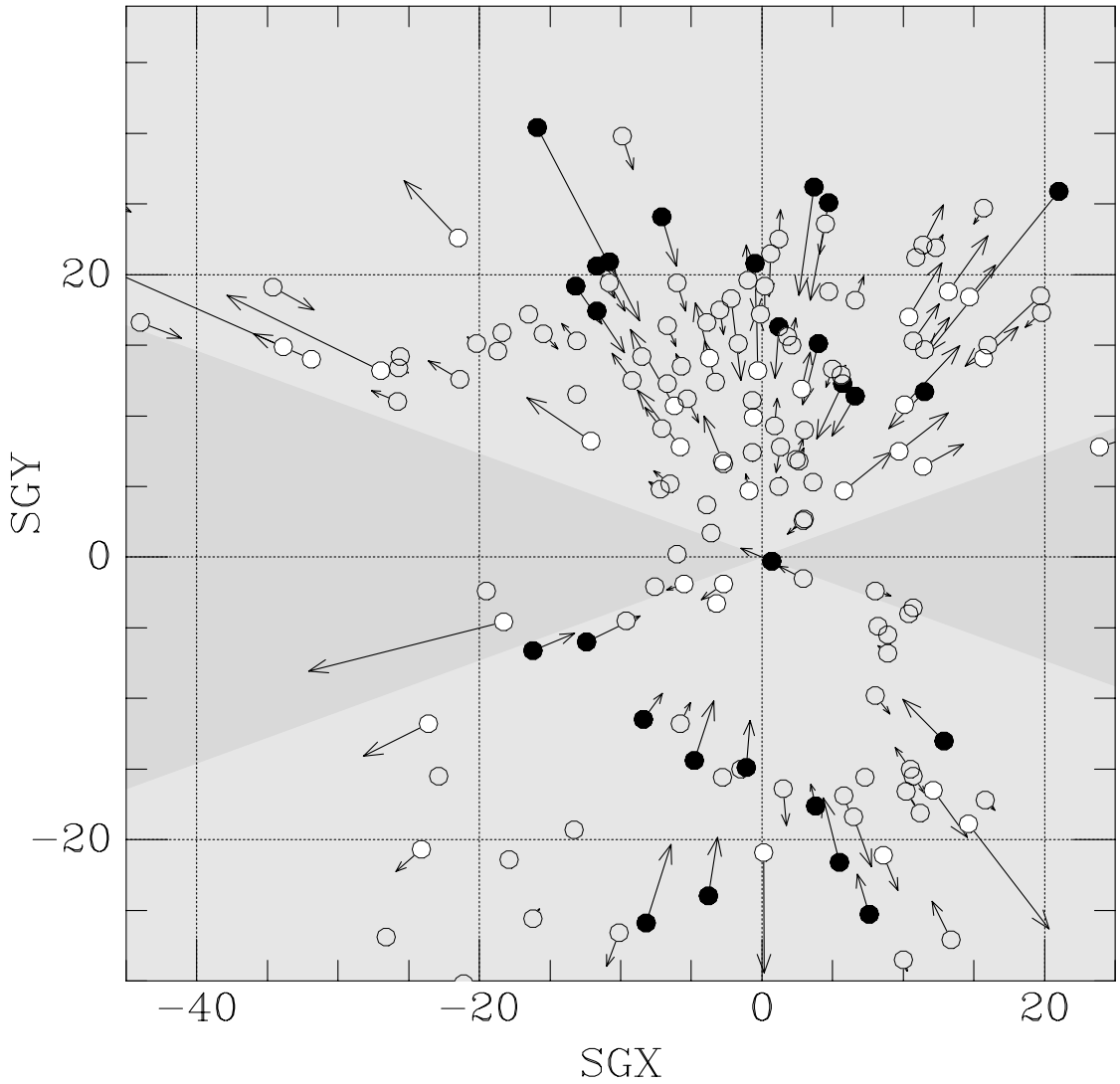

FIG. 5.—Residual velocities after removal of only a model Hubble flow and bulk flow velocity. Residual velocities which are less than 1 σ are shown as gray; greater than 1 σ are shown as black (approaching) or white (receding). For clarity only the group residual is shown for galaxies in groups.

$\sigma_{\rm VA} = 676$ km s^{-1}, and a cutoff radius $r_{\rm VA} = 9.3$ Mpc. The Hubble constant rises slightly to $H_0 = 72$, and $\boldsymbol{w} = (-320, 195, -82)$ in the CMB frame. This position for the VA is the best-fit location of a somewhat more elaborate model which also includes a Great Attractor. By itself the Virgo Attractor settles to a location of $(-3.7, 15.4, -1.7)$. The likelihood is $\mathcal{N} = 345.0$, which is a significant improvement for just three additional parameters. Figure 7 shows the residuals from this model. The "*s*-wave" of Figures 2 and 5 has been removed; the black and white points are evenly distributed around the center of the model attractor at $(-3, +16)$. However, a quadrupole signature remains evident, by which residuals in the $\pm$SGY direction tend to be blueshifted and residuals in the $\pm$SGX direction tend to be redshifted. Figure 8 shows the galaxy by galaxy residuals from this model. While they are somewhat better than Figure 6, the residual quadrupole causes substantial scatter.

The $\chi^2_N = 1.26$ value for this fit demonstrates that the model is a better match of the velocity field than a pure Hubble flow, but the evident quadrupole and the peculiar velocity in the CMB frame which misses pointing at the Centaurus cluster by only 10°, indicates a new flow in that direction. Following Lilje et al. (1986) we can add a quadrupole component to this fit, centered on the origin and with no cutoff. We find that $\mathcal{N}$ improves substantially to 320.4, and the rest of the parameters change slightly to $H_0 = 75$, $u_{\rm VA} = 132$, $\sigma_{\rm VA} = 649$, $r_{\rm VA} = 14.4$, and $\boldsymbol{w} = (-265, 200, -97)$. The quadrupole has a stretch of 6.5 km s^{-1} Mpc^{-1} in roughly the $+X/-Z$ direction, a stretch of 4.1 km s^{-1} Mpc^{-1} in the $+X/+Z$ direction, and a compression of -10.6 km s^{-1} Mpc^{-1} in the $\pm$SGY direction.

4.4. *Virgo and Great Attractor Infalls*

The above suggests that it might be profitable to try a fit with a second attractor. This is our "Great Attractor" (GA) component, and we will allow it to vary in both amplitude and position. We fit $\boldsymbol{w}$ + VA + GA in the CMB frame and find $H_0 = 73.5$, VA parameters of $u_{\rm VA} = 127$, $\sigma_{\rm VA} = 667$, $r_{\rm VA} = 14.2$, GA parameters of $u_{\rm GA} = 199$ and $r_{\rm GA} = 28.3$, centered on $(-37.7, 13.3, -18.2) \pm (1.7, 2.6, 1.6)$ Mpc, and $\boldsymbol{w} = (-146, 143, -15) \pm (79, 34, 51)$ km s^{-1}. The likelihood has improved to $\mathcal{N} = 294.9$ for 273 DOF. Figure 9 shows the residuals when this model is removed from the observed velocities, and Figure 10 shows the residual comparison. Like the previous one, this model uses power-law exponents of $\gamma = 2$ and core radii $r_c = 2$.

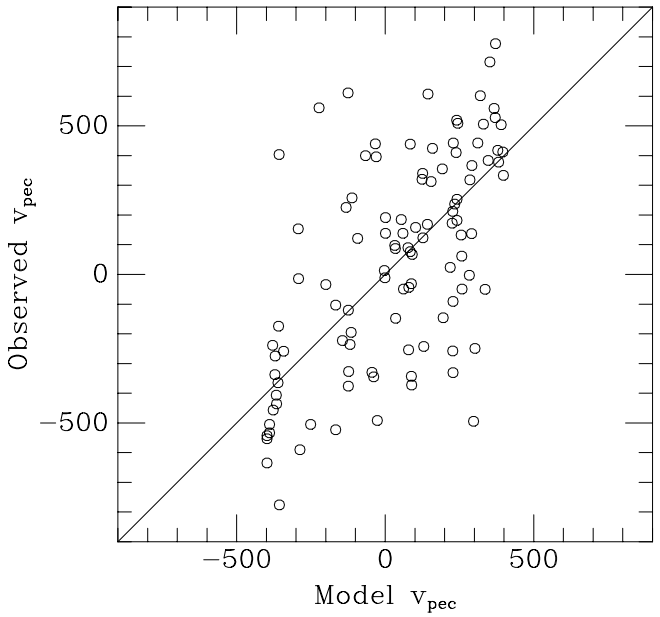

FIG. 6.—Observed peculiar velocities are compared to model peculiar velocities. Only galaxies with model velocity uncertainty less than 250 km s^{-1} {essentially $[(H_0\,\delta r)^2 + \delta v^2_{\rm virial}]^{1/2}$} are shown, thereby excluding galaxies where a significant virial velocity is expected and showing the quality of match between the model and observed large-scale flow field.

This two attractor plus dipole model appears to be a good description of the observed velocity field. It constitutes a significant improvement over a simple Virgo infall model. If we force the overall dipole to zero in the CMB frame ($\boldsymbol{w} = 0$), we find that the cutoff radii want to go to infinity, and that $\mathcal{N}$ rises to 305.3 for 278 DOF. The other parameters change quite a bit: $H_0 = 79.9$, $u_{\rm VA} = 207$, $\sigma_{\rm VA} = 675$, $r_{\rm VA} = \infty$, $u_{\rm GA} = 397$, and $r_{\rm GA} = \infty$, centered on $(-37.0,\ 16.8,\ -16.7)$ Mpc. This illustrates how sensitive some of the parameters (such as GA infall velocity) are to an assumed velocity reference frame. However, we do not have enough data out in the isotropic Hubble flow to constrain parameters with significant covariance such as w_x and $u_{\rm GA}$ to better than ~ 100 km s^{-1}. It is possible that our survey volume does have a bulk flow, but as we discuss in §§ 5.2 and 5.3 it is equally possible (and perhaps more plausible) that we have reached the limitations of what our simple parametric model can achieve.

4.5. *VA, GA, and a Quadrupole*

Finally, we return to the notion that influences from outside the volume where we have data will manifest themselves to lowest order as a dipole velocity and a quadrupole, and that our spherical flow fields are overly simplistic. We see a persistent w_y velocity and Figure 9 still seems to have a dipole pattern. We now fit a model which includes a velocity dipole, the Virgo and Great Attractors with free amplitudes and $r_{\rm cut}$, and a five component quadrupole which is centered on the origin and has a cutoff radius of $r_{\rm quad} = 50$ Mpc. We use a power-law exponent of -1.5 for the VA and -2.0 for the GA, as suggested by the confidence contours illustrated below, and $\Omega_M = 0.2$. The positions of the VA and GA are fixed at $(-3.1,\ 16.6,\ -1.6)$ and $(-36.7,\ 14.6,\ -17.1)$, respectively (their best-fit locations). We find that $H_0 = 78 \pm 3$, $u_{\rm VA} = 139 \pm 48$, $r_{\rm VA} = 12 \pm 6$, $u_{\rm GA} = 289 \pm 137$, $r_{\rm GA} = 50 \pm 44$, and $\boldsymbol{w} = (-55,\ 143,\ -8) \pm (102,\ 41,\ 62)$ km s^{-1}. Note that the large formal uncertainty on $r_{\rm GA}$ is deceptive because of its covariance with other parameters. These are illustrated in greater detail in § 4.7, where it is shown that the data want to see a steepening of the infall velocity at a distance of about 50 Mpc from the GA, but the models can achieve this over a wide range of $r_{\rm GA}$ by adjusting γ. The likelihood has improved to $\mathcal{N} = 269.2$ for 272 DOF. Figure 11 shows the residuals when this model is removed from the observed velocities, and Figure 12 shows the residual comparison. The quadrupole found by this model has an expansion of 14.6 km s^{-1} Mpc^{-1} in the $(-0.56,\ -0.16,\ +0.82)$ direction, a compression of -11.8 km s^{-1} Mpc^{-1} in the $(-0.06,\ +0.99,\ +0.15)$ direction, and a small compression of -2.8 km s^{-1} Mpc^{-1} in the $(+0.83,\ -0.04,\ +0.56)$ direction. It and the peculiar dipole $w_y = +143$ km s^{-1} are significant at more than 3 σ.

The reason that introducing a traceless quadrupole changes the model H_0 is that the sample galaxies are not isotropically distributed. In particular, the major compression axis of the quadrupole is in the direction of Virgo, which is obviously rich in galaxies. Thus, without the quadrupole component, the model is forced to compensate for this extra compression by lowering its value for H_0. It is possible that the quadrupole arises locally because discrete, spherical attractors are being used to model flows in what is actually an anisotropic potential. We discuss this idea further in § 5.2. Alternatively, the dipole and quadrupole could come from unmodeled attractors outside our volume. We investigate below whether some of the well-known galaxy superclusters such as Perseus, Coma, and Shapley could be the origin, but we will defer a more complete investigation for a subsequent paper.

4.6. *Virial Motions*

If we allow the cosmic thermal velocity dispersion to vary from the fixed value of 187 km s^{-1} that we have been assuming, we find $\sigma_{\rm cosmic} = 187 \pm 14$ km s^{-1} for our $\boldsymbol{w}$ + VA + GA + Q model, with the same model likelihood of course. This result is completely insensitive to the motions of galaxies within the Virgo cluster, as these are handled by the fitted cluster virial dispersion. Actually, this best-fit "thermal" dispersion also includes a component from the velocity measurement errors, but these are relatively small and correcting for them puts $\sigma_{\rm cosmic}$ around 180 km s^{-1}.

Our fitted value for the Virgo velocity dispersion of $\sigma_{\rm VA} \sim 650$ km s^{-1} is identical to those found in kinematical studies. The agreement is expected, since the velocity data are largely the same. For instance, Girardi et al. (1996) concluded $\sigma = 640^{+85}_{-65}$ km s^{-1} for galaxies within 2 Mpc of the Virgo core. If we delete the 12 galaxies within 2 Mpc of the center of the Virgo cluster, the fit parameters for the ($\gamma_{\rm VA} = 1.5$) model become $H_0 = 78$, $u_{\rm VA} = 139$, $u_{\rm GA} = 290$ and $\boldsymbol{w} = (-53,\ 142,\ -8)$. This is virtually identical to the model that includes the Virgo core and demonstrates that our models are able to accept large virial velocities and still reliably follow large-scale flows.

4.7. *Uncertainties, Covariances, and Constraints*

We have deliberately tried to provide a great deal of flexibility in the modeling (e.g., by always fitting for a velocity reference frame). However, there are so many parameters making up this model that it can be deceptive to quote a formal error on a parameter without disclosing the covari-

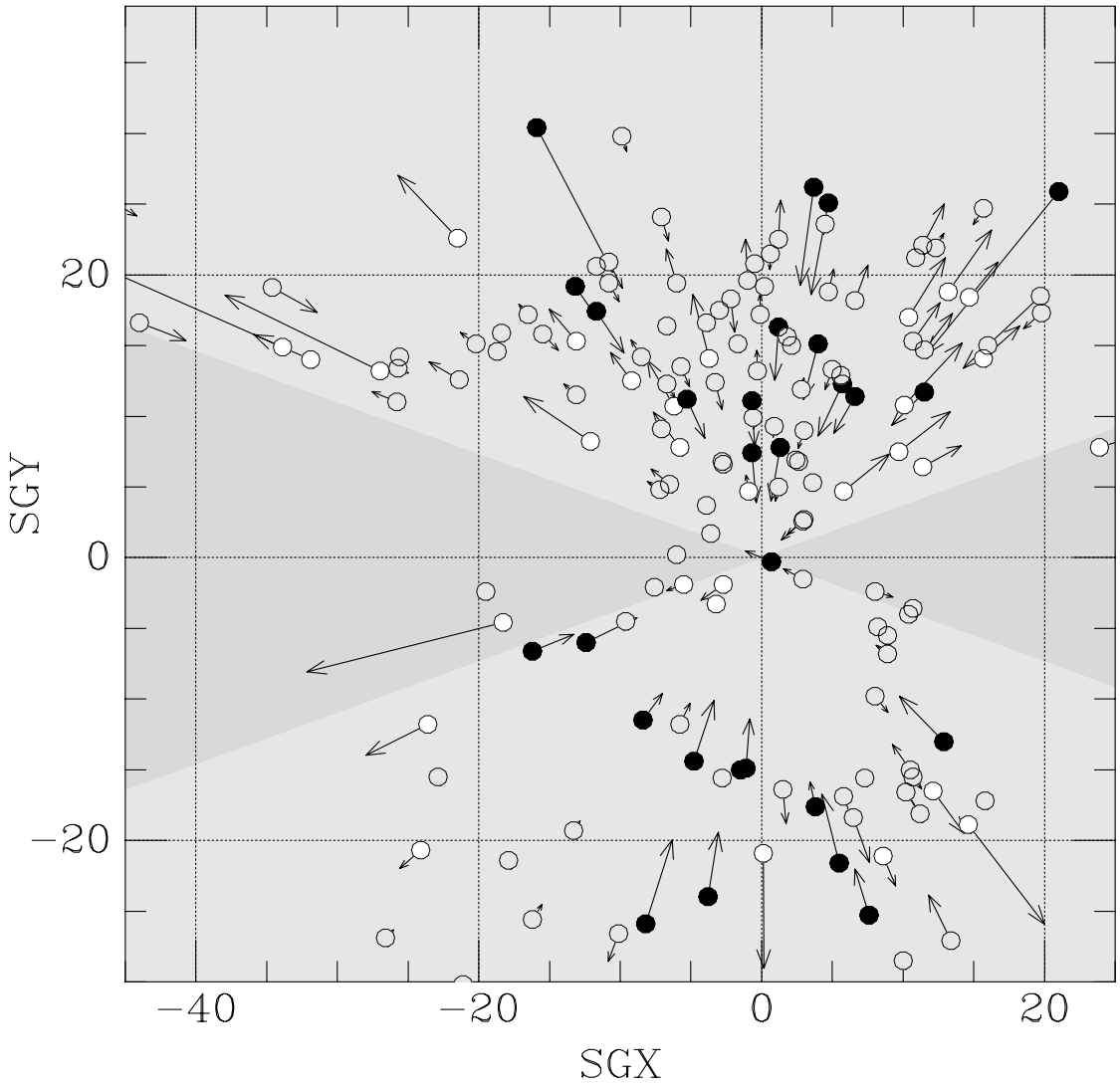

FIG. 7.—Residual velocities after removal of a model consisting of Hubble flow, Virgo Attractor, and constant velocity vector

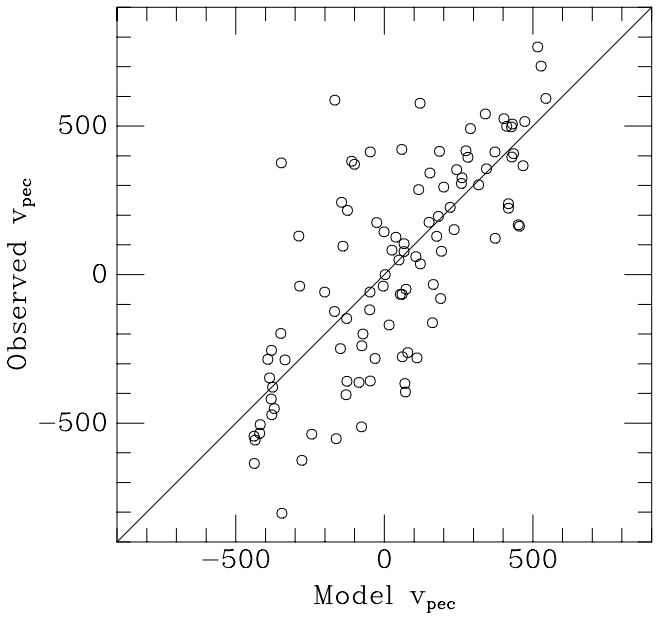

FIG. 8.—Comparison between model and observed residual velocities consisting of Hubble flow, Virgo Attractor, and constant velocity vector.

ances it has with other parameters. The greatest covariances come from the r_{cut} parameters, interacting with γ and infall amplitude especially. The next most troublesome covariances come from the SGX component of the reference frame velocity vector w mixing with the GA infall amplitude and H_0, and there is also a little bit of direct covariance between H_0 and u_{GA}. Apart from these, the formal covariances between parameters are less than 0.6 in magnitude.

The contour diagrams of this section illustrate these covariances as well as graphically showing the uncertainties in other interesting parameters. The shaded regions of these plots enclose the 68%, 90%, and 95% confidence regions for two variables, and the bars on the axes show the ± 1 σ limits for each variable considered separately. Figure 13 shows the joint confidence contours on the distance, infall velocities, and location on the sky of the Virgo Attractor, and Figure 14 shows the same thing for the Great Attractor. The locations of these attractors are evidently quite well constrained purely by the velocity data. The best-fit distance for the Virgo Attractor of 17.0 Mpc is coincident with both the location of NGC 4486 and the median of the galaxies in the core of the Virgo cluster to within the errors. We note (and describe in detail in Appendix B) that this lies

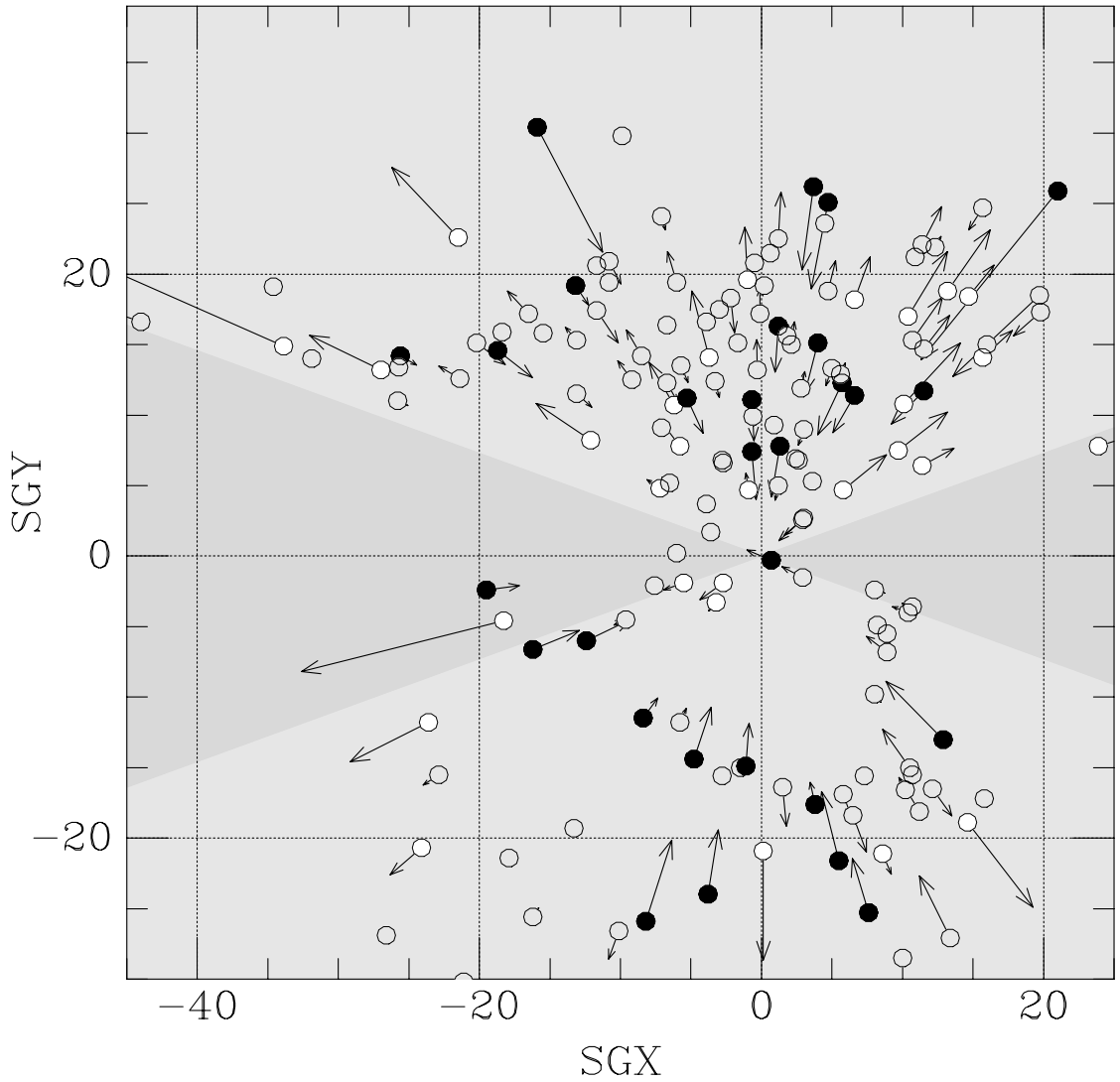

FIG. 9.—Residual velocities after removal of a model consisting of Hubble flow, Virgo and Great Attractors, and constant velocity vector

about 1 Mpc behind the mean distance of the Key Project Cepheids. The location of the GA is similar in distance to the most distant galaxies attributed to the Cen 30 cluster but lies about 15° from Cen 30. As Figure 14 illustrates, this is a complicated region.

Figure 15 shows how the SGX component w_x of the dipole velocity affects both the GA infall amplitude and the Hubble constant. The Hubble constant H_0 has a formal covariance of 0.6 with the GA infall amplitude, but such a small covariance scarcely affects the determination of each independently.

Figures 16 and 17 show the confidence contours for the Virgo and Great Attractors, of the $r_{\rm cut}$ parameter and the power-law exponents, and of $r_{\rm cut}$ and the infall velocities. Evidently, these parameters are very poorly constrained individually, and values of $0 < \gamma < 2$ for VA and $1 < \gamma < 3$ for GA can be offset by appropriate changes in $r_{\rm cut}$ to yield acceptable models. Nevertheless, overall run of peculiar velocity with position varies little among these models.

Figure 18 shows the run of net model velocity as a function of position along vectors toward the Virgo and Great Attractors. The curves are $\gamma = 0.1$, 1.5, 3, and $r_{\rm cut} = 5$, 12, ∞ (VA) and $\gamma = 1$, 2, 2.5, 3, and $r_{\rm cut} = 15$, 50, ∞, ∞ (GA) for which $\mathcal{N}$ is virtually constant around 269. (The enclosed density profile of the Virgo Attractor can be described quite accurately as an exponential with scale length 5 Mpc.) Except in the cores of the attractors, the curves differ very little. We also plot the galaxies which lie within 25° of the vectors ($|\cos\theta| > 0.9$) to give a sense of the number of constraining points we have near the attractors (although the attractor models are affected by galaxies all over the sky). The agreement between the galaxy and model velocities in this plot should only be very approximate close to the attractors because the angle between the line of sight and the vector from the galaxy to the attractor becomes much greater than 25°.

Figure 19 illustrates this slightly differently. These panels show how $u_{\rm infall}$ for each of the two attractors individually varies as a function of distance from the attractor, given these four models with very different γ-values. The models diverge close to and far from the attractors, but there is a broad range where the models give substantially the same values for infall velocity ($6 < r < 25$ Mpc for the VA and $10 < r < 50$ Mpc for the GA). We draw power-law approximations for these two attractors on the plots whose slopes are -1.1, although it is apparent that all models for both

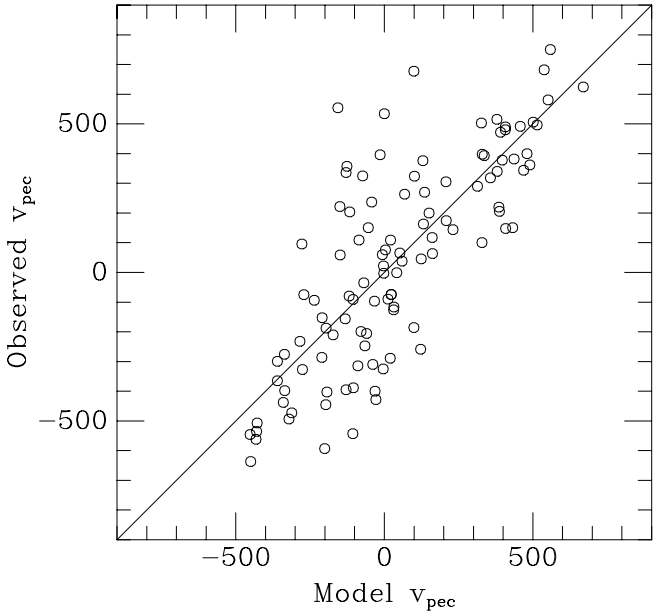

FIG. 10.—Comparison of velocity residuals after removal of a model consisting of Hubble flow, Virgo Attractor, GA, and constant velocity vector.

attractors curve away from a pure power law over these radial ranges. The ratio of attractor infall velocity to Hubble flow is for the Virgo Attractor

$$\frac{u_{\rm VA}}{H_0 r} = 0.11\left(\frac{r}{r_{\rm VA}}\right)^{-2.1} \tag{13}$$

and for the Great Attractor

$$\frac{u_{\rm GA}}{H_0 r} = 0.09\left(\frac{r}{r_{\rm GA}}\right)^{-2.1}, \tag{14}$$

where $r_{\rm VA}$ and $r_{\rm GA}$ are the distances of the Local Group from the attractors.

Not surprisingly, for a given value of Ω_M we find quite consistent values for δ, the overdensity within our radius, for these models. For the Virgo Attractor, values of $0.1 < \gamma < 3$ lead to values of $\delta = 1.0 \pm 0.07$, or $M_{\rm VA} = 7 \times 10^{14}\ M_\odot$. However, if the quadrupole is caused by a nonspherical Virgo (as we suggest below), these estimates for δ and $M_{\rm VA}$ are not meaningful, although equation (13) is. For the Great Attractor, models with $1 < \gamma < 3$ lead to values of $\delta = 0.73 \pm 0.14$, or $M_{\rm GA} = 9 \times 10^{15}\ M_\odot$. (These masses, of course, are the masses in excess of background density within spheres centered on the attractors with

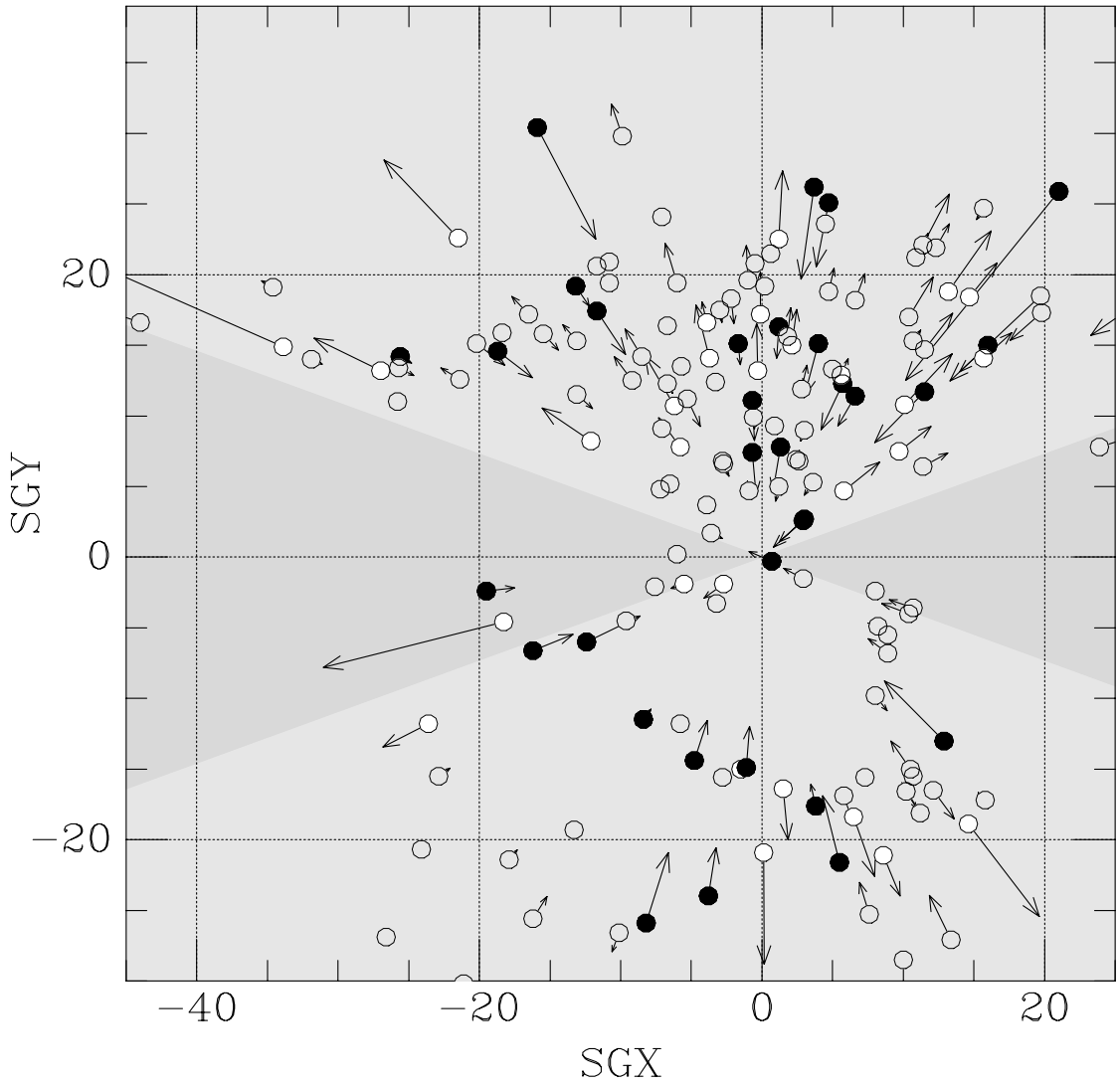

FIG. 11.—Residual velocities after removal of a model consisting of Hubble flow, Virgo and Great Attractors, constant velocity vector, and quadrupole

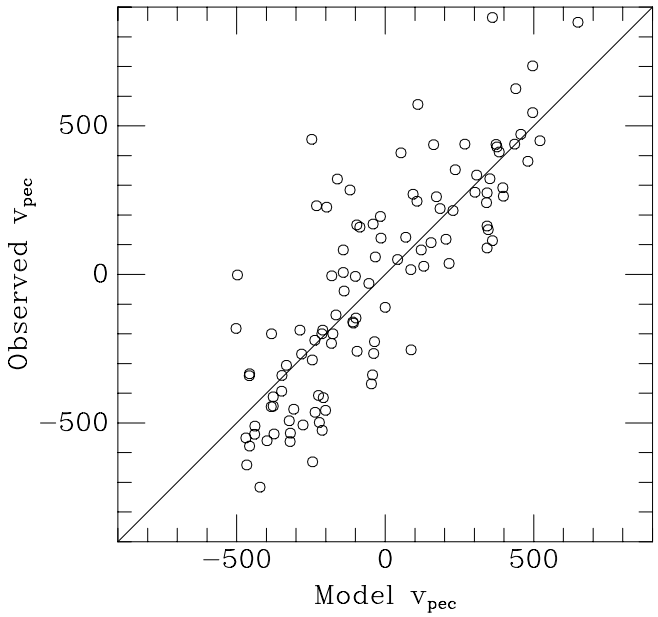

FIG. 12.—Comparison of velocity residuals after removal of a model consisting of Hubble flow, Virgo and Great Attractors, constant velocity vector, and quadrupole.

radius reaching the Local Group.) From this it is easy to solve for the radius and angle subtended by the zero velocity surface (sphere where infall cancels outward Hubble flow) around these attractors. For the Virgo Attractor this is 6 Mpc, or 20°; for the GA it is 14 Mpc, or again about 18°. We see from Figure 19 that by $\delta \approx 1$ ($u/H_0 r \approx 0.1$) the models do not fit well unless they are falling at least as steeply as r^{-3}. In particular, pure isothermal models ($\gamma = 2$, unmitigated by any cutoff) would provide poor representations of the mass distributions.

The GA distance is well constrained in these models at $d_{GA} = 43 \pm 3$ Mpc. This is a bit behind most of the galaxies comprising the Cen 30 and Cen 45 clusters. In fact, the Cen 30 "cluster" appears to be galaxies distributed over 5–10 Mpc on the near side of the GA and the "*s*-wave" distortion of the Hubble flow causes them to share similar redshifts. This is illustrated in Figures 20 and 21, which show contours of our flow model with and without survey galaxies overlaid. We do not have a good constraint on the GA amplitude closer than 10 Mpc, so the very dramatic peculiar velocities inside that radius may well be overestimates. In this projection, the Centaurus galaxies fall above the GA, but they lie in the "stall" region (where projected infall compensates for Hubble flow and radial velocity varies little with distance) near $\pm 15°$ angular separation, and the model and data agree on a typical CMB velocity of 3150 km s^{-1}. Similarly, the Ursa Major group lies in the stall region near the VA with a CMB velocity of 1150 km s^{-1}, and the Virgo Southern extension lies in a stall zone with CMB velocity of 1500 km s^{-1}. The general trend of the model for v_{CMB} to range from 1100 to 1500 km s^{-1} as SGL swings from 85° to 125° is apparent in redshifts surveys of the region, as is illustrated in Figure 22.

We note that the GA distance increases by about 10% when the three high-velocity Cen 45 galaxies (with good quality data) are included in the modeling. However, the likelihood of the model suffers badly in trying to accommodate just these three additional DOF, rising from $\mathcal{N} = 269$ to $\mathcal{N} = 295$. Thus, for now we have chosen to exclude them. A detailed discussion of the distribution and motions of galaxies in the GA/Centaurus region, and a comparison of the SBF flow model results with those of previous GA models will be given by Dressler et al. (2000).

4.8. *Influence of Perseus-Pisces and Shapley*

We now ask if the Perseus-Pisces supercluster and/or the Shapley Concentration could be sources of the peculiar dipole $\boldsymbol{w}$ and quadrupole that we find. To test this idea, we add to our standard $\boldsymbol{w}$ + VA + GA + Q model compact attractors representing Perseus-Pisces at (65, −15, −17) and Shapley at (−170, 120, −30), allowing the masses to be free parameters. The likelihood $\mathcal{N}$ improves to 267.2, which

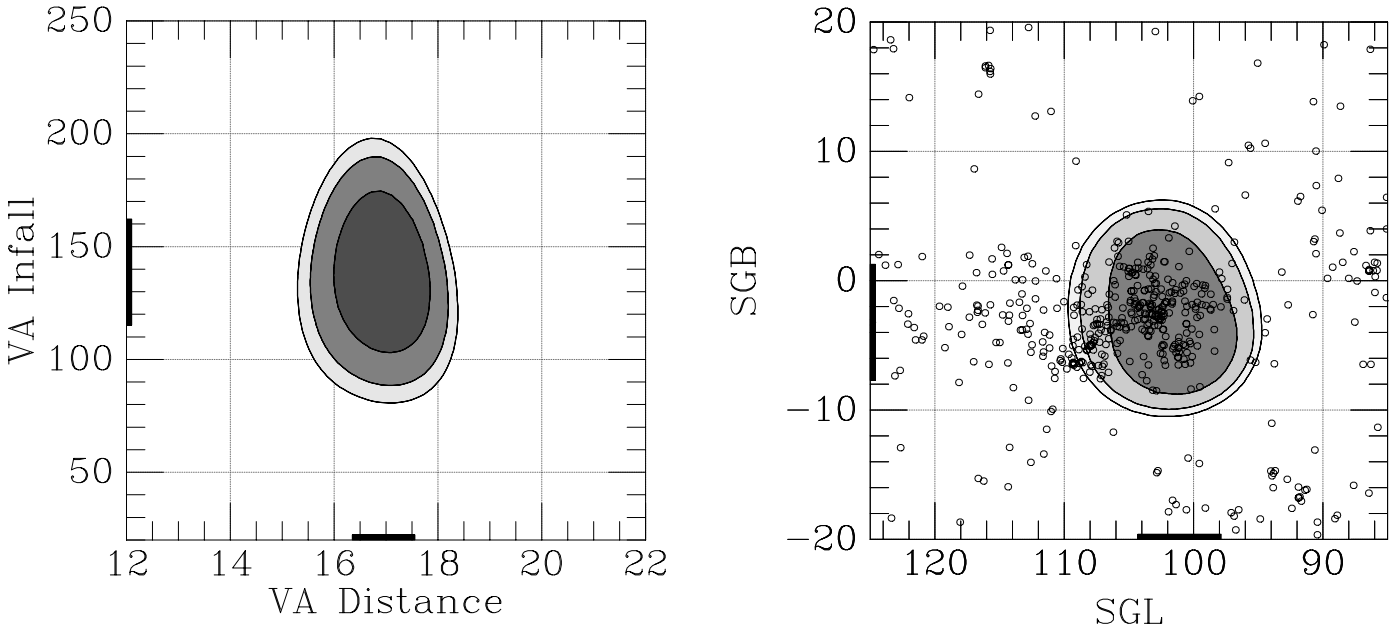

FIG. 13.—Joint confidence contours of the fitted infall velocity, distance, and location of the sky of the Virgo Attractor. The points show the location of the galaxies in the RC3 with $v_h < 2800$.

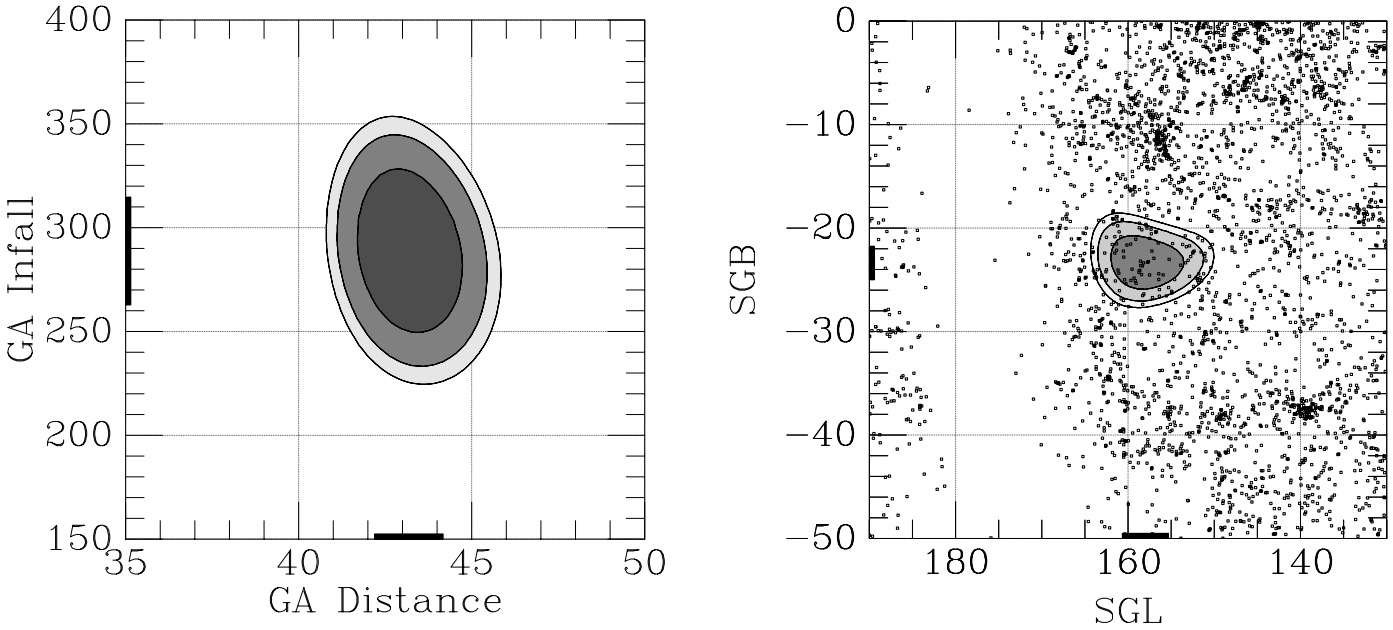

FIG. 14.—Joint confidence contours of the fitted infall velocity, distance, and location of the sky of the GA attractor. The points are from the SPS survey; Centaurus lies at (156, −12), Abell 1060 is the cluster at (139, −37), and the Galactic plane is evident on the left side.

is not a significant improvement for two new parameters over the previous value of 269.2. For Perseus-Pisces, we find an insignificant velocity amplitude of $v_{\rm amp} = 59 \pm 314$ km s^{-1}; recall that this is normalized at the fiducial radius of 50 Mpc. For Shapley, we find an unbelievable amplitude of $v_{\rm amp} = 17{,}926$ km s^{-1}, which corresponds to a velocity of 1013 km s^{-1} at the Local Group for the assigned distance of 210 Mpc. The other parameters must change a great deal to compensate for this, especially w which adjusts itself to (920, −530, 210). Equally telling however, is the fact that the quadrupole *grows* to have eigenvectors of 22, −20, and −2 km s^{-1} Mpc^{-1}, indicating that the inclusion of Perseus and Shapley has made this model less plausible.

There is a great deal of covariance between the distant Shapley attractor and the w term, so we ran another model including the Shapley attractor but with w set to zero. This model gave a velocity amplitude $v_{\rm amp} = 2533 \pm 717$ km s^{-1}, corresponding at the Local Group to 144 ± 41 km s^{-1}. The likelihood of this model is $\mathcal{N} = 274.0$, which for only one additional parameter is a substantial improvement over the $\mathcal{N}$ of 278.5 found for a model with VA + GA + Q but no w or Shapley component. However, the fit is worse than our standard model with w and no distant attractors, although the difference in the fitted quadrupole components for these two models is now insignificant. (Adding a Perseus attractor gives no further improvement; it is in the wrong direction to compensate for the lost flexibility of w.)

We conclude that Perseus-Pisces exerts no significant influence on our local volume, consistent with previous

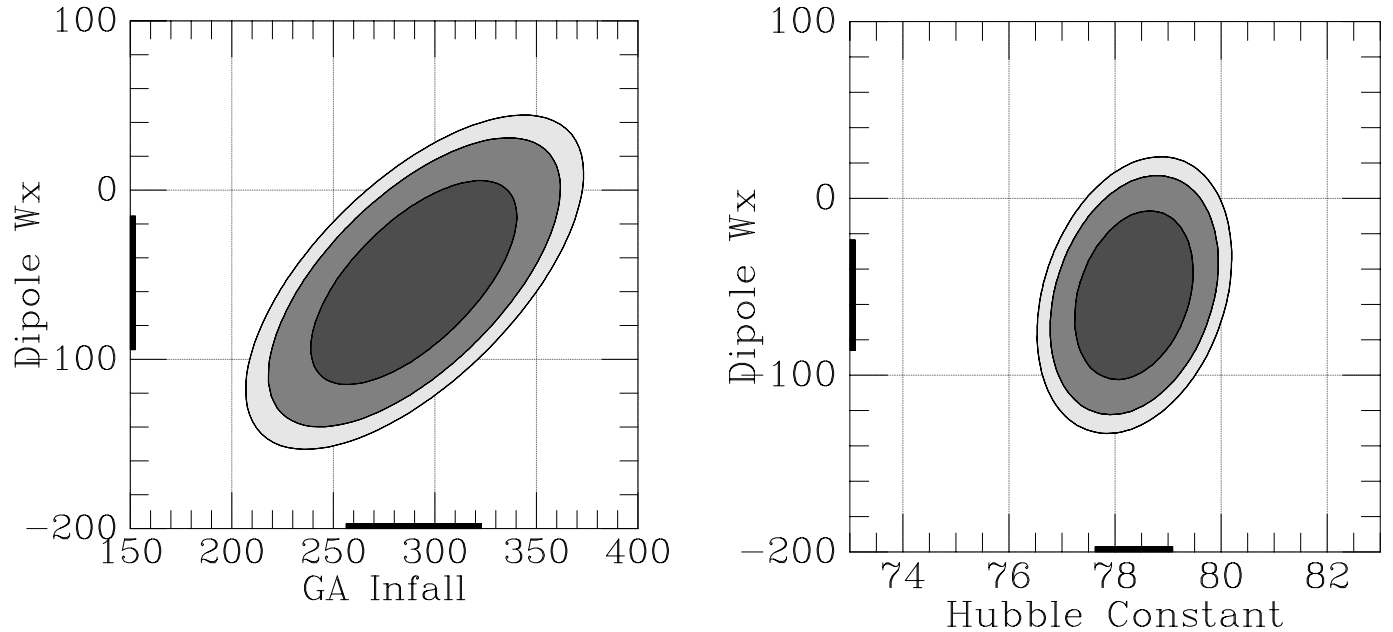

FIG. 15.—Joint confidence contours of the SGX component w_x of the dipole velocity with GA infall amplitude (*left*) and H_0 (*right*)

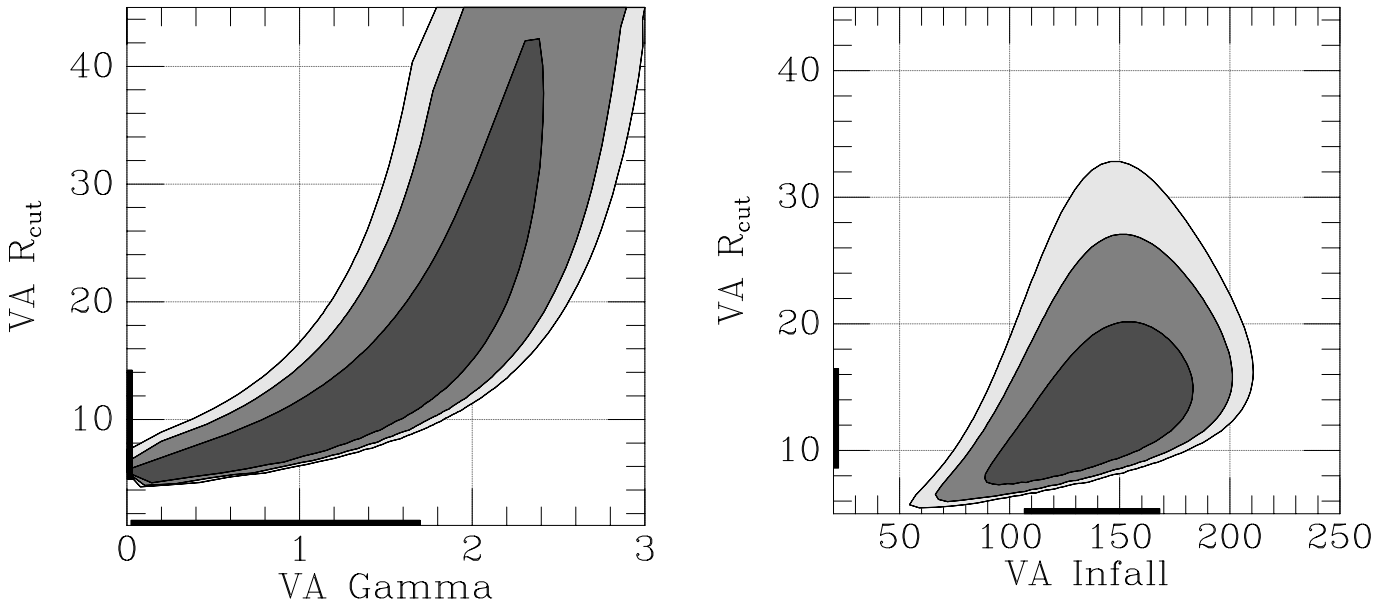

FIG. 16.—Joint confidence contours of the cutoff radius r_{cut} and power-law slope γ (*left*) and infall amplitude (*right*) for the Virgo Attractor

studies in this direction (e.g., Willick 1990; Courteau et al. 1993; Hudson et al. 1997), and that the Shapley Concentration is not the source of the peculiar quadrupole in our modeling, although it might contribute some part of the observed dipole. Bearing this last point in mind, we continue with our standard model because it provides a better fit to the data than the model which replaces $\boldsymbol{w}$ with a Shapley attractor. In addition, we show below in § 5.2 that the dipole can be removed by simply translating the quadrupole origin to the center of Virgo.

Similarly, we experimented with including nearby Abell clusters, selected under the assumption that their galaxy counts are proportional to their masses and ranking them by M/r^2. Using a suite of the 22 most significant ones (including Coma, Perseus, A2199, etc.) and allowing their mass-to-luminosity ratio to be a free parameter gives a likelihood $\mathcal{N} = 268.8$, not a significant improvement. The model parameters are virtually unchanged, including the quadrupole and the dipole velocity.

4.9. Ω_M

Lacking any a priori information about the values of δ, we have very little constraint on Ω_M. Only the nonlinear component to Yahil's $\rho^{1/4}$ law (eq. [4]) provides any leverage at all. Nevertheless, if we permit Ω_M to be a free parameter the best-fitting model comes in with $\mathcal{N} = 269.2$, and $\Omega_M = 0.08 \pm 0.33$. If we refit our standard model with $\Omega_M = 1$, we find $\mathcal{N} = 269.5$, again indicating how little direct handle we have on Ω_M. The other parameters change very little, but as expected, the combination of $\delta\Omega_M^{2/3}$ for the two attractors is relatively constant for the various values of Ω_M at 0.33 for the Virgo Attractor and 0.27 for the Great

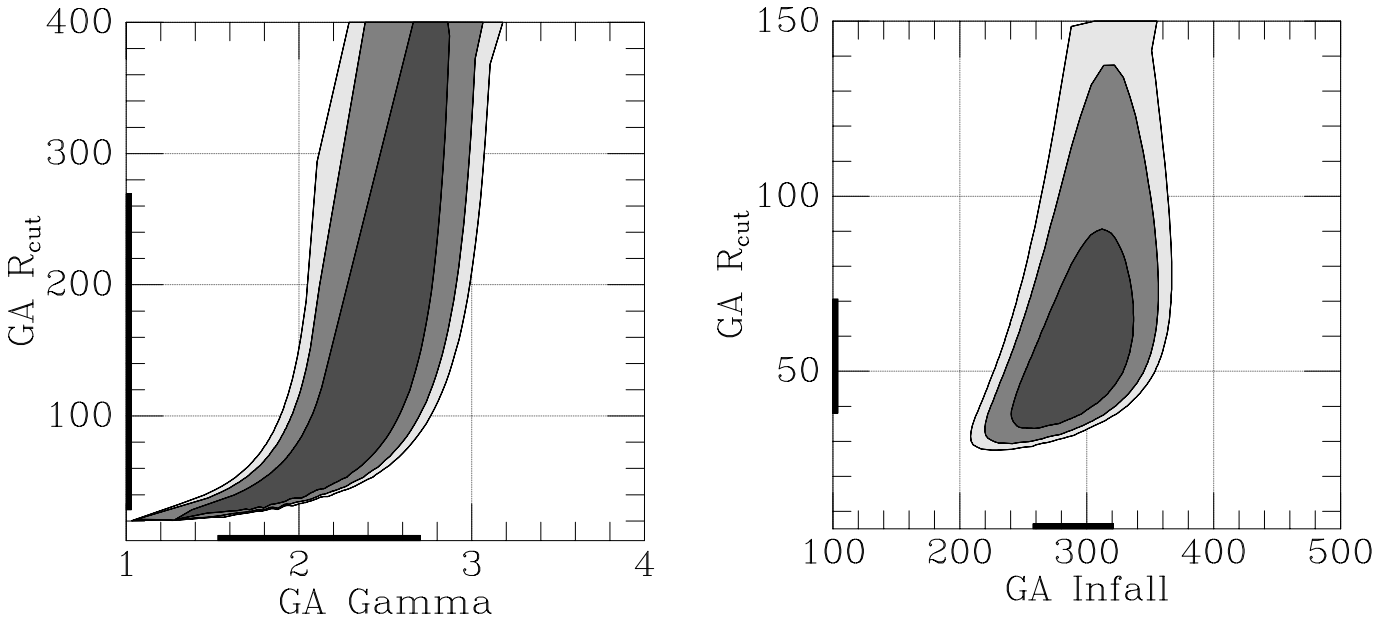

FIG. 17.—Joint confidence contours of the cutoff radius r_{cut} and power-law slope γ (*left*) and infall amplitude (*right*) for the GA attractor

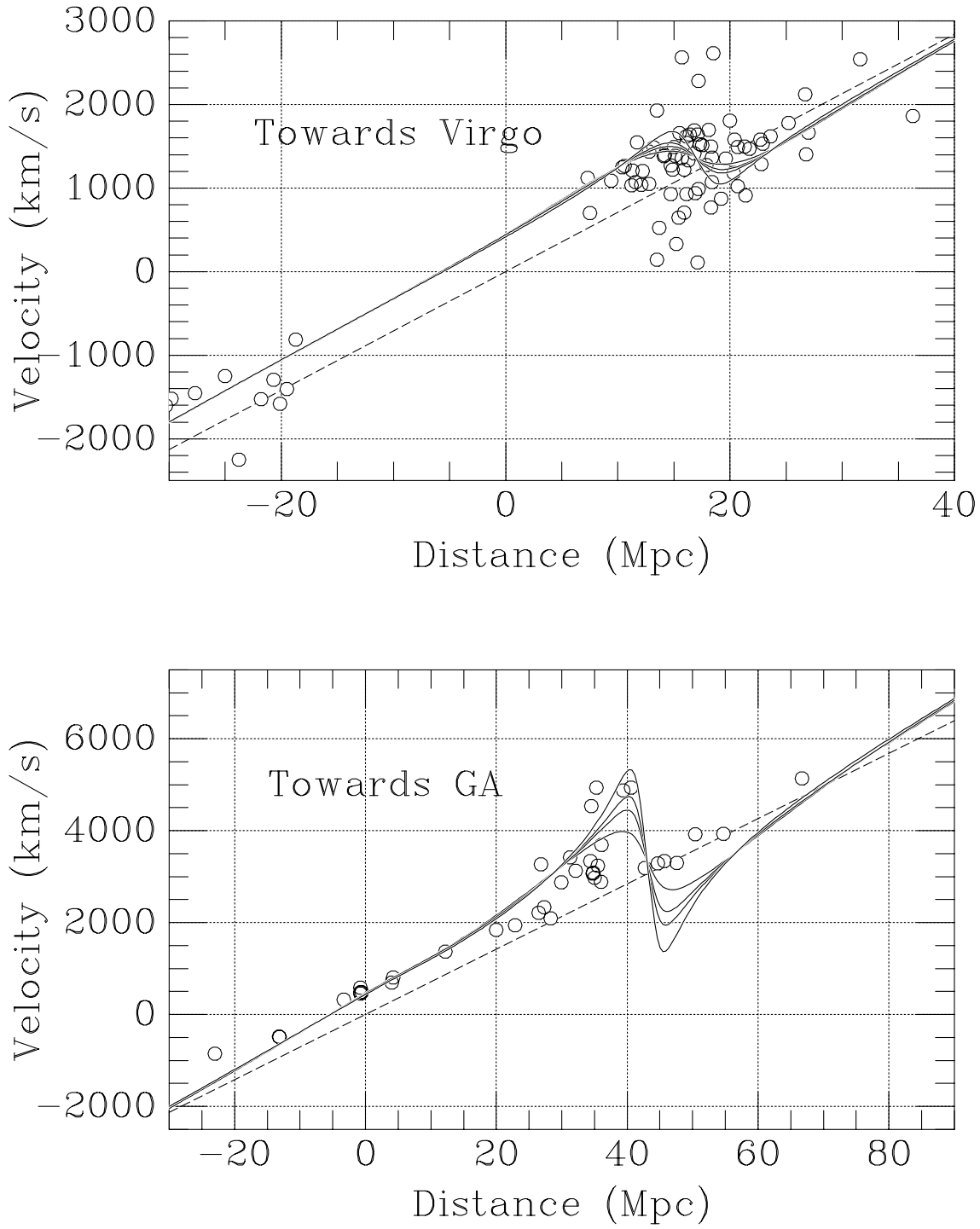

FIG. 18.—Net model velocity is shown as a function of position along vectors running through the Virgo and Great Attractors using various values of γ and $r_{\rm cut}$ which leave $\mathcal{N}$ constant. The dashed line is just $H_0 r$. The points are those galaxies within 25° of the vectors ($|\cos\theta| > 0.9$).

Attractor. We note that an initial comparison our measured peculiar velocities to the galaxy distribution of the *IRAS* 1.2 Jy flux-limited redshift survey finds $\Omega_M = 0.24 \pm 0.05$ (Blakeslee et al. 1999b), assuming the *IRAS* galaxies are unbiased tracers of the mass distribution.

5. DISCUSSION

5.1. *Mass Distributions of the Virgo and Great Attractors*

We find good fits to the velocity field using attractors whose density distributions go as $\rho \sim r^{-2}$ when r is small enough that $\delta > 1$, but steepening to $\rho \sim r^{-3}$ by $\delta \approx 1$. Most previous parametric flow models have adopted isothermal $\gamma = 2$ attractors (e.g., Lynden-Bell et al. 1988; Han & Mould 1990), as γ was not well constrained by their data sets. Aaronson et al. (1989) did allow γ to vary in their model, although they constrained it to be the same for both the Virgo and Great Attractor mass concentrations, and found $\gamma \approx 2$. Faber & Burstein (1988) also experimented with different values of γ and found that Virgo was roughly

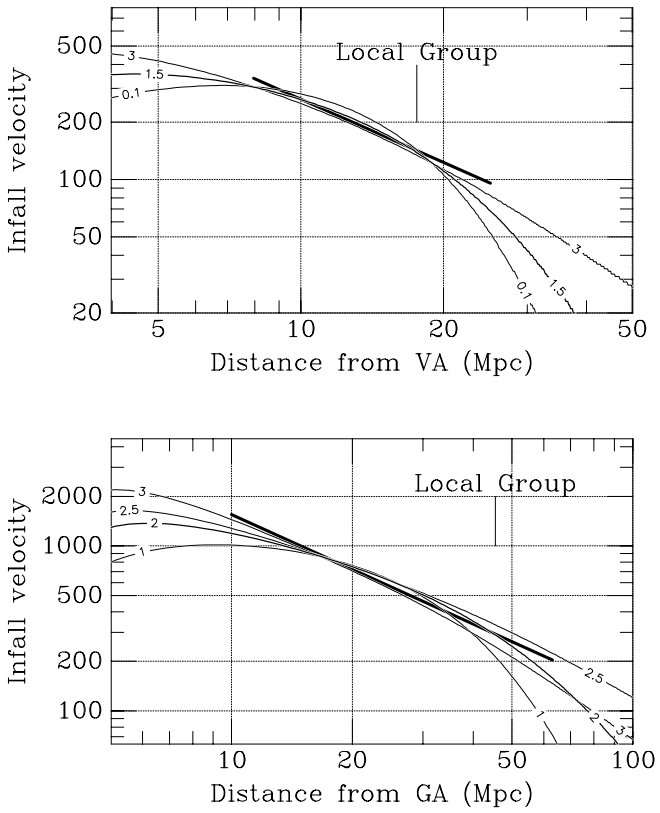

FIG. 19.—Model infall velocity is shown as a function of distance from the Virgo and Great Attractors for different values of γ. The solid line delineates the range where there is substantial agreement and where we believe the models are well constrained by the data.

isothermal, and the more distant GA preferred $\gamma \sim 2.7$. This is similar to what we find with $r_{\rm cut}$ set to infinity and γ allowed to vary, but we prefer the approach adopted in the previous section because of the substantial improvement of the fit.

The assumption of isothermal cluster mass distributions in these early flow studies was motivated largely by analogy to the Milky Way and the evidence that cluster mass-to-light ratios increase outward from the core (e.g., Faber & Gallagher 1979), as well as by theoretical modeling (e.g., Blumenthal et al. 1986). Observations do show fairly flat velocity dispersion profiles for many clusters, in support of this assumption (e.g., Fadda et al. 1996). Weak lensing observations are also consistent with isothermal, or somewhat steeper, mass distributions (Squires et al. 1996a, 1996b). However, none of these studies probes beyond a few Mpc from the cluster centers, whereas we are dealing here with the distributions over tens of Mpc.

Numerical studies by Navarro, Frenk, & White (1996, 1997) suggest that cluster dark matter halos in hierarchical collapse models should go as r^{-3} at large radii. Earlier numerical work on the collapse of isolated halos produced even steeper r^{-4} profiles at large radii (Dubinski & Carlberg 1991). The total mass of course depends strongly on γ, with the $\gamma \leq 3$ yielding an infinite mass; thus at some point the distribution must steepen. Our observed mass profiles therefore are quite reasonable in terms of flat velocity dispersion profiles and the numerical simulations.

5.2. *Dipoles and Quadrupoles*

Although we find a 4 σ, 150 km s^{-1} dipole residual pointing in the SGY direction, we regard this result as an indication that our survey volume, which extends to about 3000 km s^{-1} or 40 Mpc, is essentially at rest with respect to the CMB. Indeed, we can clearly create or remove any dipole velocity we like by shifting the origin of the quadrupole contribution, as is evident from equation (5), provided the quadrupole matrix is invertible. Applying the inverse of the quadrupole to the dipole velocity $\boldsymbol{w}$ of our best-fit model implies a quadrupole origin of $(-17, 13, -9)$, rather close to the VA, although moved somewhat toward the GA. If we shift the quadrupole origin from the Local Group to the center of the Virgo Attractor (which can then partially mimic the effects of a flattened attractor), choose a cutoff $r_{\rm quad} = 35$ Mpc, and fit with $\boldsymbol{w} = 0$, we find $\mathcal{N} = 272.0$, which is only 3 greater with effectively three fewer degrees of freedom; it is 6.5 less (with the same DOF) than the model with $\boldsymbol{w} = 0$ and the quadrupole centered on the LG. Alternatively, we can fit for $\boldsymbol{w}$ with the quadrupole centered on the Virgo Attractor, and we find $\boldsymbol{w} = (-91, -7, -63)$ or within 1 σ of zero in each coordinate. We therefore think it likely that the galaxies in our survey volume are on average at rest with respect to the CMB, and that the dipole and quadrupole terms of our standard model are acting as lowest order correction terms to our spherical Virgo Attractor.

We found previously that addition of a quadrupole component to the two attractor model caused the Hubble constant to increase from 73 to 78 as the likelihood improved. This is illustrated in the left panel of Figure 23, which shows confidence contours of our standard model as a function of H_0 and quadrupole amplitude relative to the best-fit value. We find that moving the origin of the quadrupole to Virgo also has a slight side effect on the value of the Hubble constant. If there were no cutoff in the quadrupole, its origin would be completely degenerate with $\boldsymbol{w}$, but when the quadrupole is centered on Virgo we find that H_0 drops slightly to 76, and there is some covariance between H_0 and $r_{\rm quad}$ in the sense that larger $r_{\rm quad}$ leads to larger H_0, as seen in the right panel of Figure 23. Because this use of a quadrupole correction to a spherical infall model seems like a poor approximation to a flattened potential, and because the eigenvectors of the quadrupole are tipped by 45° from the SGZ symmetry axis of the galaxy distribution, we do not prefer this model over the one which has the quadrupole centered on the Local Group. Nevertheless, we are mindful of the sensitivity of H_0 to this possibility, and we therefore choose $H_0 = 77 \pm 4$ as the most likely range we can derive from these data and models.

Unlike Lynden-Bell et al. (1988), we do not find that Centaurus has a much larger radial peculiar velocity in the CMB frame than the Local Group. Instead it appears to have a significant extent falling into the attractor at 43 Mpc and at least some galaxies (e.g., NGC 4767) have no radial velocity with respect to the CMB. Dressler et al. will discuss this issue in greater depth, but it appears that the flow in the Great Attractor region is fairly complex and may need many more high accuracy distances before it can be completely untangled.

5.3. *Motion of the Local Group*

The Local Group is moving at 627 km s^{-1}, with com-

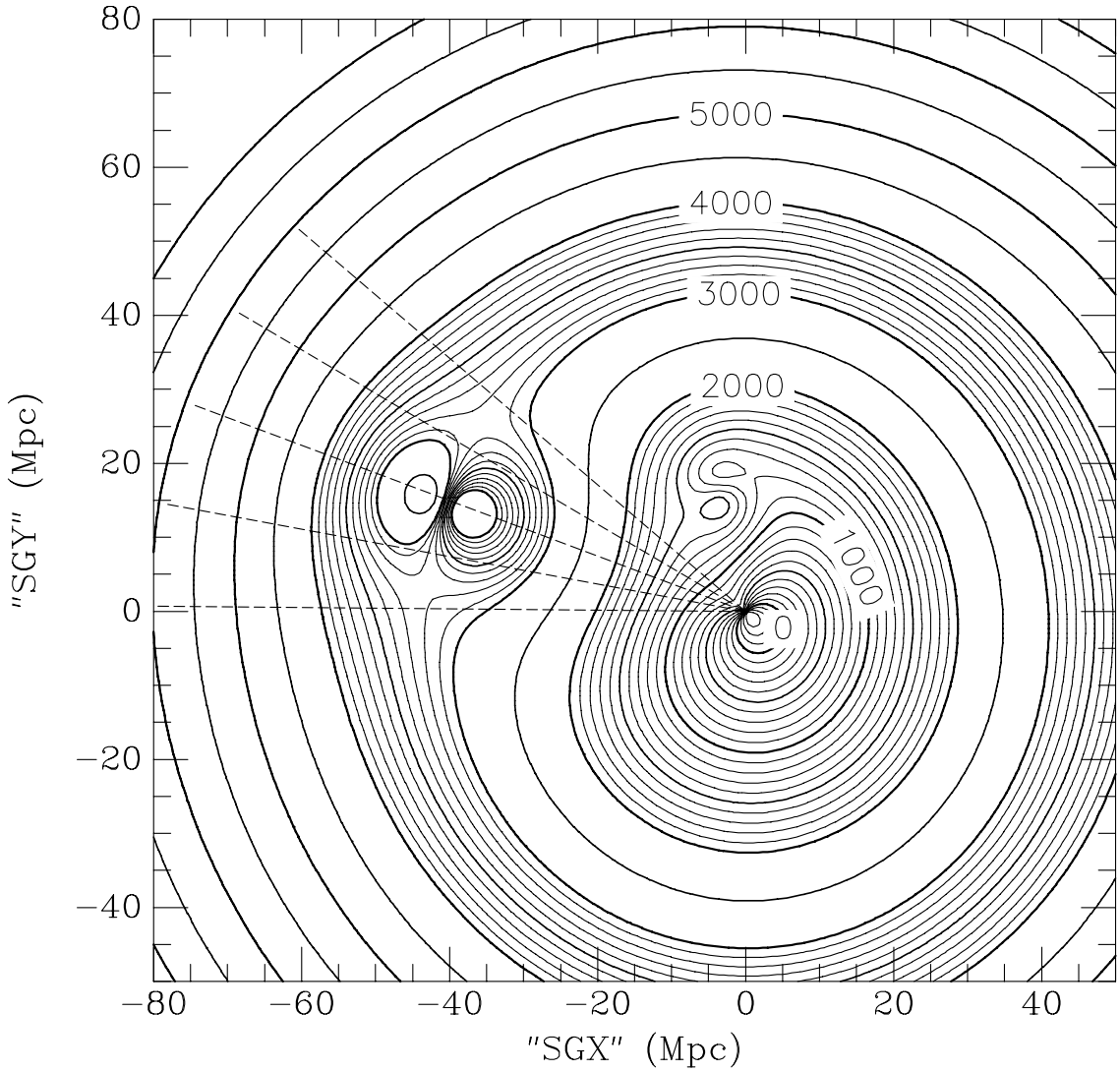

FIG. 20.—Contours are shown of our model of the radial component of the flow field in a plane which cuts through the Local Group, Virgo, and Great Attractors. The model velocity of the Local Group with respect to the CMB frame is apparent in the discontinuity at the origin. The Virgo Attractor is found at "SGX, SGY" = (−3, +17) (quotes because the plane does not correspond perfectly to supergalactic coordinates); the Great Attractor is at (−42, +16), and radial lines are drawn at ±10° and ±20° from it.

ponents (−406, 352, −324) km s^{-1}, with respect to the CMB frame, but we have not used this fact at all in our modeling. To what extent can we account for this motion of the Local Group reference frame in the context of our model? The three contributors to the model velocity at the Local Group are as follows:

$$W = -55, 143, -8\ ,$$
$$\text{Virgo} = -25, 136, -13\ ,$$
$$\text{GA} = -247, 98, -115\ ,$$
$$\text{Net} = -327, 377, -136\ ,$$
$$\text{Obs} - \text{net} = -79, -25, -188\ .$$

We can account for w_x and w_y quite well; the residual of −79 km s^{-1} is not statistically significant and is in any case a reasonable peculiar velocity for the Local Group with respect to the nearby flow field.

The w_z residual of −188 km s^{-1} is much too large to be an unsuspected motion of the Milky Way with respect to the LG frame. The models by Yahil et al. (1977) and Courteau & van den Bergh (1999), among others, require that this be a motion of the entire Local Group. Our sample does not have any nearby galaxies which are far enough out of the supergalactic plane to ascertain whether this motion is restricted to the Local Group or extends farther. The nearest galaxy in our sample with |SGB| > 20° is 8 Mpc distant, and at SGB = −33° we could not distinguish between $v_z = 0$ and $v_z = -188$. We note that this velocity is similar in magnitude to our best-fit one-dimensional thermal velocity.

This peculiar motion of the Local Group in the general direction of −SGZ has been noted before and was named the "Local Anomaly" (LA) by Tully (1988) and Faber & Burstein (1988), who both attributed it to inhomogeneities in the galaxy distribution within $cz \sim 1000$ km s^{-1}, including the "Local Void" (Tully & Fisher 1987). These authors found fairly large LA velocities: the Faber & Burstein value was 360 km s^{-1} toward (l, b) = (199°, 0°), or (169, 30, −317) km s^{-1} in supergalactic components. Han & Mould (1990) modeled the LA in more detail and found a smaller net motion of 236 km s^{-1} toward (l, b) = (205°, 11°), or (88, 68, −208) km s^{-1}. All three of these sets of authors used the Aaronson et al. (1982b) infrared Tully-

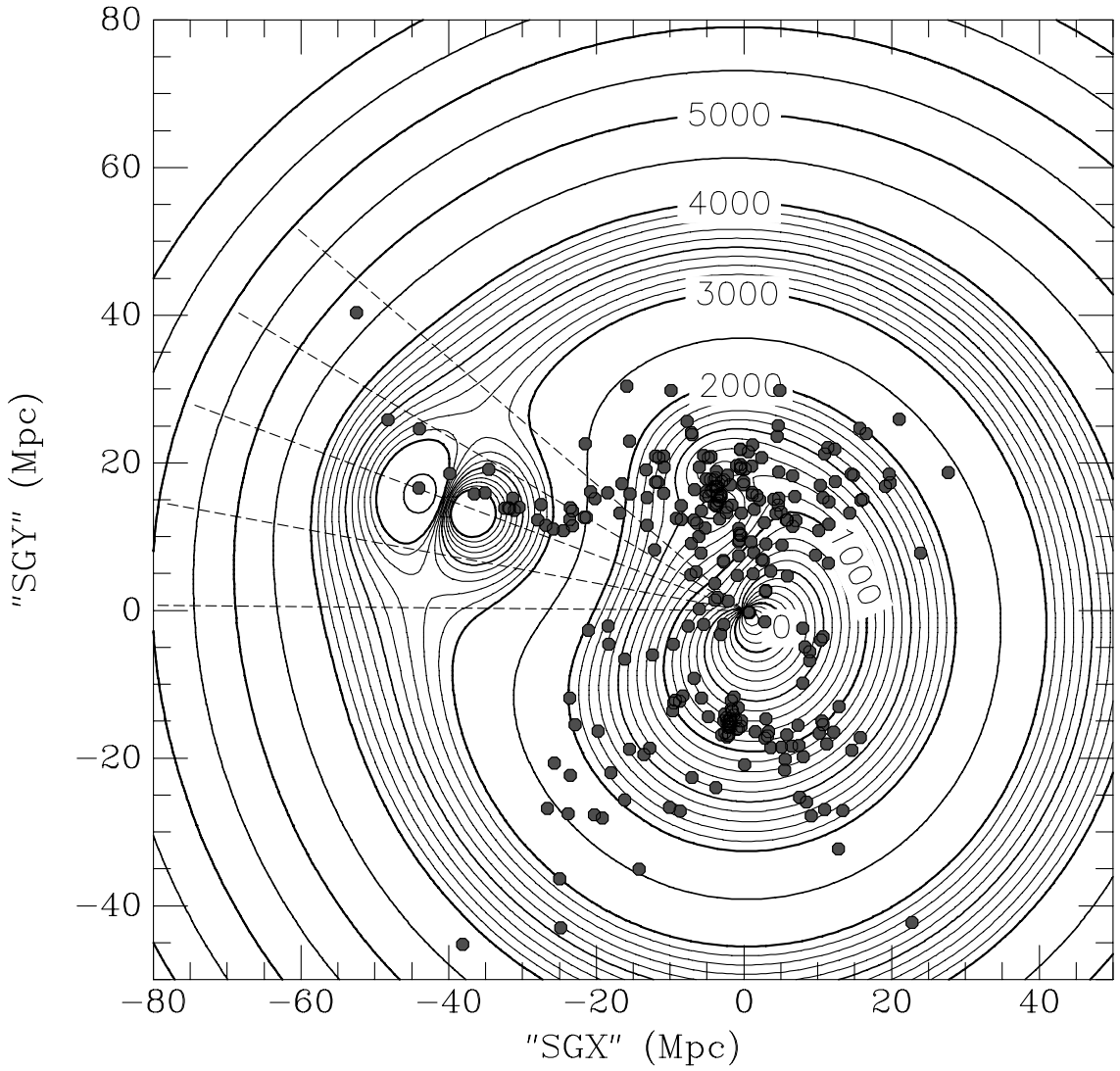

FIG. 21.—Same as Fig. 20, except that our survey galaxies are overplotted. Note that the Centaurus galaxies that appear to be going through the Great Attractor actually pass above it by about 15°, and hence, lie in the stall zone.

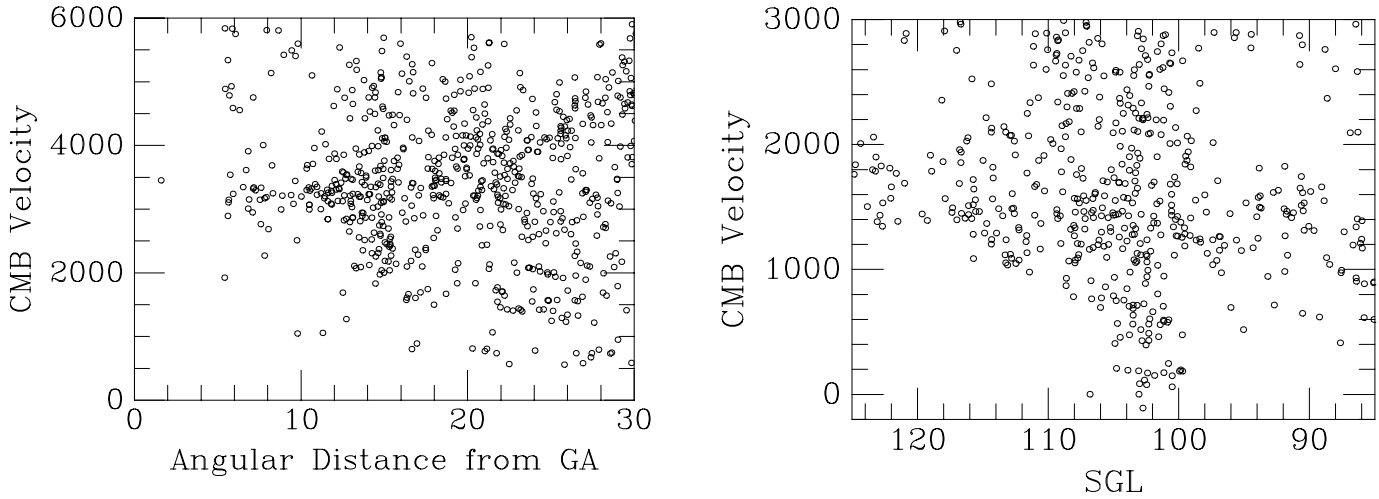

FIG. 22.—CMB velocities of galaxies from the RC3 are plotted as a function of angular separation from the GA (*left*), and as a function of supergalactic longitude SGL (*right*). The concentration at $v_{\rm CMB} = 3150$ (*left*) and the trend for $v_{\rm CMB}$ to change from 1100 to 1500 km s^{-1} (*right*) inherent in our model is apparent in these redshift data.

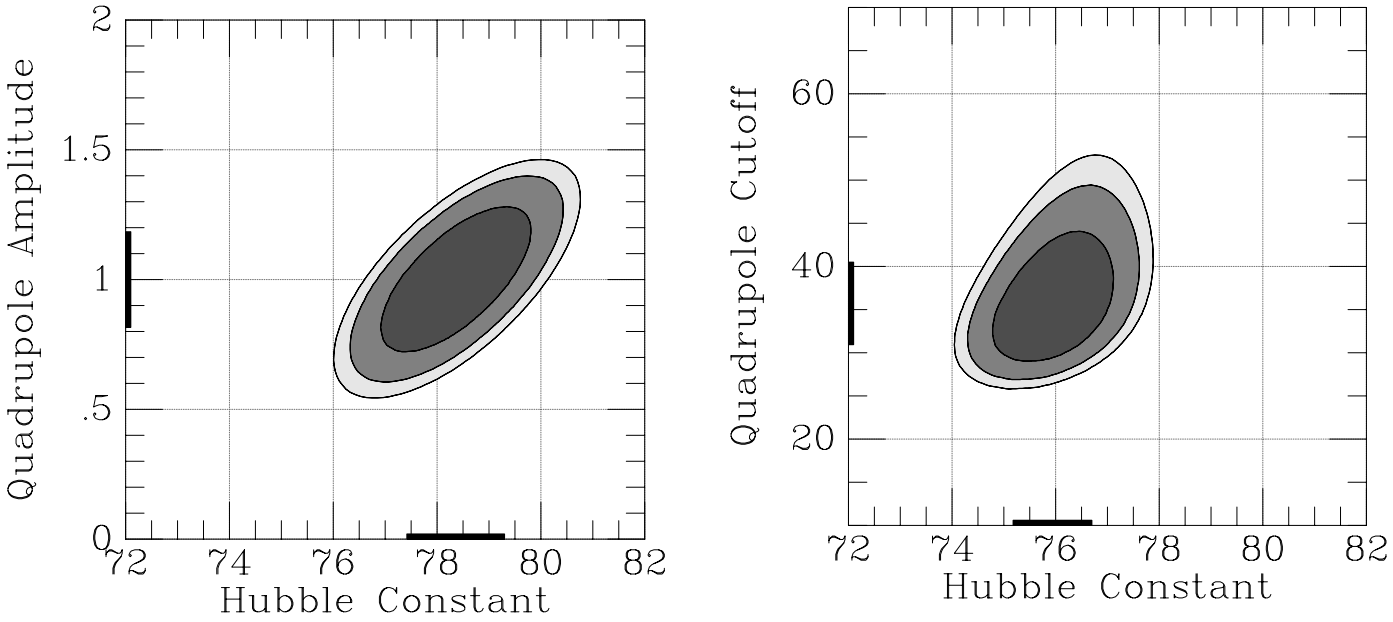

FIG. 23.—Joint confidence contours of the Hubble constant and relative quadrupole amplitude when the quadrupole is centered on the Local Group are shown on the left. Confidence contours of Hubble constant and quadrupole cutoff radius when the quadrupole is centered on Virgo instead are displayed on the right.

Fisher data set to measure the LA. Aaronson et al. (1982a) themselves found a LG peculiar motion of (38, 86, −150) km s^{-1} and attributed the large −SGZ velocity to a displacement of the Local Group above the supergalactic plane and a resultant downward acceleration.

Lahav et al. (1993) suggested that the LA could be explained by the combined effects of the Local Void in the +SGZ direction and the Puppis concentration of galaxies toward −SGZ, with possible smaller contributions from Fornax and Eridanus. The Puppis concentration was revealed by H I surveys of *IRAS*-selected galaxies; it is a rich, but loose, association of galaxies lying in the Galactic plane at $(l, b) = (245°, 0°)$ with a mean velocity of about 2000 km s^{-1} (Yamada et al. 1994). Lu & Freudling (1995) surveyed the region behind the Galactic plane toward the direction of the Faber & Burstein (1988) and Han & Mould (1990) LA vectors and disputed the conclusion of Lahav et al. Since they found no other significant excesses of nearby galaxies, Lu & Freudling concluded that any motion arising from a gravitational pull of nearby galaxies and a push from the Local Void, whose center is nearly diametrically opposite Puppis, would have to be directed almost straight toward Puppis, nearly 45° from the supposed direction of the LA vector.

In fact, the Local Anomaly we find here has an apex at $(l, b) = (250°, -13°)$, remarkably close to the direction of the Puppis concentration and to the anticenter of the Local Void as sketched out by Lu & Freudling. However, the magnitude we find is significantly smaller than the Faber & Burstein value adopted by Lahav et al. (1993); thus, the ∼50 km s^{-1} contribution they estimated for the Puppis galaxies becomes less necessary. Likewise, Han & Mould (1990) concluded that the Local Void might account for their fairly modest LA motion, if the mean position of the Void was a free parameter.

We experimented with adding a Gaussian void, as defined by equation (8), to our standard model along the positive SGZ axis. We first looked at a very small Local Void with both the distance and Gaussian size set to 10 Mpc and fitted for the velocity amplitude. Since there is some covariance between $v_{\rm amp}$ and w_z, we set $w_z = 0$. We find a best-fit amplitude of $v_{\rm amp} = -8.5 \pm 5.6$ km s^{-1}, and an improvement in $\mathcal{N}$ from 269.2 to 267.7, marginally significant. This void provides a push of −65 km s^{-1} at the location of the LG. The model parameters show little change, although H_0 drops from 78 to 77 km s^{-1} Mpc^{-1}. Alternatively, we tried adding a Local Void using the distance and size of 20 Mpc suggested by redshift surveys and fixing the amplitude at the value of $v_{\rm amp} = -88$ km s^{-1} which provides the push of −188 km s^{-1} at the Local Group that we are trying to understand. The central δ of this void is close to −1. This time we do allow w_z to vary. The fit improves still more to $\mathcal{N} = 265.9$ and w_z is still negligible at 20 km s^{-1}, but the amplitudes of the VA and GA shift quite a bit to 172 and 159 km s^{-1}, respectively, w_x and w_y also move to −136 and +151 km s^{-1}, and H_0 decreases to 73 km s^{-1} Mpc^{-1}. Obviously, fine-tuning the free parameters could produce an even better match to the excess LG motion, but this is precisely the sort of ad hoc modeling which we think is not appropriate. This void's properties are not well constrained in our model, nor are there well-motivated external constraints, so we choose not to make this adjustment to our standard model, but simply note that our peculiar velocity data do seem to support the idea that there is a 20 Mpc void above the Local Group which is nearly empty at its center.

Another interesting issue is the peculiar velocity of the Local Group with respect to the Virgo Attractor, since this was the historical means of determining the Virgo infall amplitude. The Local Group is approaching Virgo at about 139 km s^{-1} due to the Virgo Attractor itself; the Great Attractor causes the LG and Virgo to converge at 97 km s^{-1}; the extra quadrupole component results in the LG and Virgo approaching each other at an additional 173 km s^{-1}. The total model peculiar velocity between the Local Group and Virgo is therefore 409 km s^{-1}.

It is unclear how much "infall velocity" to ascribe to the Virgo Attractor. Using our model of the Virgo Attractor as

a spherical distribution, it only tugs on us at 139 km s^{-1}. However, if we regard the entire quadrupole as a component of an anisotropic Virgo Attractor, the net tug on the LG is 312 km s^{-1}. These considerations may partially account for the widely disparate values which have been reported for the Virgo infall amplitude. Depending on the sample one is using and whether one's fit is dominated by model amplitudes near our location or averaged all around the Virgo supercluster, it is possible to get naive "infall velocities" (i.e., peculiar velocity between Virgo and the LG) anywhere between 140 and 400 km s^{-1}.

5.4. *Comparison with Other Flow Studies*

Our analysis finds more modest infall velocities at the Local Group and a smaller bulk flow than most previous studies. Part of the reason for our smaller infall velocities is that our modeling has been more flexible in not requiring a single power-law profile for the massive attractors. Thus, our model can accommodate fairly large infalls close to the attractors without requiring large motions at the Local Group. In addition, we have not required the spherical infalls to account for all of the Local Group motion in the CMB frame, but rather have allowed the reference frame to be a free parameter. In fact, setting $w = 0$, $r_{\rm cut} = \infty$, and omitting the quadrupole term yields a model similar to that of Lynden-Bell et al. (1988) but at a significant cost in the likelihood (see § 4.4).

Our best-fit bulk flow w of $\sim$150 km s^{-1} toward $(l, b) = (294°, +67°) \pm 43°$, and the strong indications that even this modest value may be an artifact of the model, appears inconsistent with several recent studies which find large-scale streaming motions of amplitude $\sim$700 km s^{-1} for volumes encompassing our survey volume (e.g., Lauer & Postman 1994; Hudson et al. 1999; Willick 1999). However, it is quite consistent with the bulk flows found by the *I*-band Tully-Fisher study of Giovanelli et al. (1999) (using their "Case b" weighting). These authors report bulk flows of 151 ± 120 km s^{-1} toward $(l, b) = (295°, +28°) \pm 45°$ for their full sample of 24 clusters extending out to 9000 km s^{-1}, and 131 ± 90 km s^{-1} toward $(l, b) = (325°, +62°) \pm 60°$ for their 17 clusters within 6000 km s^{-1}.

Our best-fit one-dimensional thermal velocity is $\sigma_{\rm cosmic} = 180 \pm 14$ km s^{-1}, after making allowance for velocity measurement uncertainty. Lynden-Bell et al. (1988) found a best-fit thermal dispersion of 250 ± 40 in their favored model and concluded that this result was mainly due to small-scale flows, not virial dispersions in groups.

Strauss, Cen, & Ostriker (1993) calculated the thermal velocity dispersions from several peculiar motions surveys in order to compare the resulting Mach numbers (the ratio of the mean bulk flow to the three-dimensional thermal dispersion) to expectations from various cosmologies. Their estimates of the one dimensional dispersions from the observational surveys ranged from 250 to 420 km s^{-1}. More recent large-scale flow studies often simply assume a value $\sigma_{\rm cosmic} = 250$ km s^{-1} for clusters and find that the resulting $\chi^2_N \sim 1$ (e.g., Willick 1999; Hudson et al. 1999). The Giovanelli et al. (1999) cluster study allowed this to be a free parameter and found $\sigma_{\rm cosmic} = 300 \pm 80$ km s^{-1}. However, on small enough scales there is evidence that the dispersion of galaxies (field spirals in particular) about their local flow field is closer to $\sim$125 km s^{-1} (Davis, Miller, & White 1997; Willick et al. 1997). This value may better reflect the virial velocities of galaxies within small groups.

5.5. *The Revised Calibration and H_0*

The revised $\overline{M}_I$ calibration of equation (2) carries a formal zero-point uncertainty of 0.10 mag from the SBF/Cepheid galaxy comparison. This uncertainty is larger than the 0.07 mag quoted in SBF-I because that paper used the group comparison, which averaged many SBF distances for each Cepheid distance. As described in Appendix B, the group comparison is 0.13–0.19 mag fainter than the galaxy comparison. By choosing the galaxy calibration over the group one, we have implicitly assumed that the difference is due to a systematic offset in the mean distances of the *HST* Key Project Cepheid galaxies and the groups in which they are thought to reside. The alternative explanation is that the measured SBF magnitudes are systematically too bright for the spiral bulges, either because of population effects or because of extra variance from dust or other features. Ferrarese et al. (1999) have likewise chosen the former explanation and have derived a calibration similar to that given here.

With this new calibration and depending on the flow model, we have derived values of H_0 in the range of 70–80 km s^{-1} Mpc^{-1}. This range correlates with the amount of mass in the model attractors. The value of $H_0 = 70$ corresponds to a pure Hubble flow plus overall dipole model; at the other extreme with $H_0 = 80$ is a dual isothermal ($\gamma = 2$) attractor model with $r_{\rm cut}$ set to infinity. The former model is ruled out by the extremely poor χ^2_N; the latter model overestimates the attractor masses, thus overestimating H_0. When we allow $r_{\rm cut}$ to vary and produce an r^{-3} (and steeper) large radius falloff to the models, H_0 comes out near 74. There is, however, a significant degree of anisotropy in the data with respect to this model as evidenced by the dramatic improvement in likelihood when a quadrupole component is introduced into the model. As it happens, relieving this anisotropy with a quadrupole centered on the Local Group causes our value for H_0 to rise somewhat to 78, whereas a quadrupole centered on Virgo yields an H_0 of 76. Despite our qualms about the ad hoc nature of the latter model, the fact that it has a w consistent with zero causes us to prefer it slightly for estimating H_0. Thus, for our best estimate of a flow-corrected but unbiased value, we adopt

$$H_0 = 77 \pm 4 \pm 7 \text{ km s}^{-1} \text{ Mpc}^{-1} . \quad (15)$$

The first error bar is the quadrature sum of the internal uncertainty for a single flow model and an estimate of the likely range from the different models. The second error bar includes the 0.10 mag uncertainty in the fitted calibration to Cepheids and an estimated 0.17 mag uncertainty in the Cepheid zero point itself (see Ferrarese et al.); these systematic uncertainties also have been combined in quadrature.

Our value for H_0 differs from the value of 69 km s^{-1} Mpc^{-1} found by the Ferrarese et al. (1999) analysis of SBF partially because of our choice of zero point and partially because of the flow models used. We have done extensive modeling to estimate and remove the effects of large-scale flows from our data. Another difference is that we have used the full survey data set in deriving H_0, rather than just four SBF measurements from *HST*. Consequently, our best value is 11% larger than theirs, although marginally consistent within the random uncertainty.

Blakeslee et al. (1999b) have recently compared the same peculiar velocities measured in our survey with the predictions from the galaxy density field measured in the *IRAS*

and ORS redshift surveys. In contrast to the present work, the only free parameters in the density field comparison are $\beta \equiv \Omega^{0.6}/b$, where b is the linear biasing factor, and H_0. The most consistent results from that work are obtained with $H_0 \approx 74$, somewhat lower than the result obtained here. As Blakeslee et al. suggest, this may be due to our decision to omit the poorly defined (in a parametric sense) local void, which as we have seen has the effect of lowering H_0 due to the local underdensity. However, we regard the very close similarity between the density field H_0 and that obtained here as encouraging evidence that the flow field presented here is reasonably accurate.

As with the Key Project results, if the Cepheid calibration is changed so that the distance modulus of the Large Magellanic Cloud is 0.2 mag smaller than the standard 18.5 mag value, then H_0 would increase by 10%; if the Kennicutt et al. (1998) metallicity dependence for the Cepheid period-luminosity relation is correct, then H_0 would decrease by 5%. However, our calibration would become quite discordant with the theoretical calibration using Worthey's models if the zero point moved by more than about 0.2 mag, and those models are largely based on the RR Lyrae and parallax distance scales, rather than Cepheids.

6. SUMMARY AND CONCLUSIONS

We have shown that the SBF technique is a powerful tool in mapping the local and large-scale velocity field through accurate distance measurements to early-type galaxies. Judging by our best data, for which the product of seeing and distance PD < 1, distance measurements with an accuracy of $\pm 5\%$ are attainable for any early-type galaxies with sufficiently good data. Distance measurements of this accuracy are essentially immune to Malmquist-like biases.

The parametric model we have developed is unique in the way it handles both local peculiar motions and velocity dispersions, particularly for galaxy clusters. Although it is important to follow this first analysis with nonparametric models, we find it remarkable that nearly all of the deviation from a smooth Hubble flow can be accounted for by the addition of two spherical, truncated power-law attractors, one centered on the Virgo cluster and the other centered just beyond the most distant of the ellipticals associated with the Cen 30 and Cen 45 clusters. These two attractors appear to center on enhancements in galaxy distribution, consistent with the idea that galaxy light traces mass in at least some approximate way. The improvement in the model with the inclusion of an additional dipole and quadrupole is statistically significant, but our analysis indicates that these terms are more likely the result of inadequacies in the spherical attractor model, rather than manifestations of additional mass fluctuations beyond our survey volume. Further measurements, particularly beyond the $R \approx 40$ Mpc limit of most of our data, will be able to discriminate between competing explanations, but it is clear from the size and direction of these components that the influence of mass overdensities in the Perseus-Pisces supercluster or Shapley concentration do not play a substantial role in perturbing the velocity field within 3000 km s^{-1}.

Not surprisingly, we find strong covariance between pairs of parameters, for example, the amplitude of the GA infall and the strength of the dipole component in this direction, or the cutoff radius and the power-law exponent of mass distribution attributed to the attractors. New data are unlikely to reduce some of these covariances, but additional measurements on the backside of the Great Attractor, for example, will be able to constrain much better the contribution from more distant concentrations that produce a local dipole.

Our standard flow model resolves most of the Local Group's motion with respect to the CMB, except for the continued presence of a nearly 200 km s^{-1} component perpendicular to the supergalactic plane. This "Local Anomaly" has been seen before in other data sets. The amplitude we find is generally smaller than in those previous studies, and crude modeling of this "anomalous" motion as a "push" from a nearby void in the +SGZ direction can account for nearly all of it.

Our data are considerably more accurate than those used in the analysis of Lynden-Bell et al. (1988). Our best-fit model, while qualitatively similar, is significantly different, but this is mainly a product of our inclusion of other components, for example, the inclusion of a dipole in addition to the two attractors. In particular, the thermal velocity of our sample is only 180 km s^{-1}, significantly lower than the Lynden-Bell et al. study. A more detailed comparison of our study with previous results will appear in Dressler et al. (2000).

We find zero or at most a very small dipole motion in the $R < 3000$ km s^{-1} volume, which is consistent with the study of Giovanelli et al. (1999), mildly inconsistent with the larger bulk flow reported by Courteau et al. (1993), and very inconsistent with the large-amplitude, large-scale flows reported by Lauer & Postman (1994), Hudson et al. (1999), and Willick (1999) unless the $R < 3000$ km s^{-1} volume is at rest with respect to the CMB while the thick shell with $3000 < R < 10{,}000$ km s^{-1} is rapidly moving, a situation we think is very unlikely.

Finally, we provide a new zero point for the SBF relation, based on SBF distances to galaxies that have Cepheid distances determined by the *HST* Key Project. The Hubble constant that results from this calibration, $H_0 = 77 \pm 4 \pm 7$ km s^{-1} Mpc^{-1} is somewhat higher than results of that study, partially because we choose a different zero point and partially because we have a more extensive set of galaxies and a more sophisticated model. We consider the zero point issue to be unresolved and in need of further study.

Our study shows the power of accurate SBF distance measures in advancing our understanding of the local mass distribution and the distortions in the velocity field that result from it. Extending the SBF technique, through bigger aperture telescopes with better PSF performance, through near-IR SBF measurements, and through observations with *HST* and future space telescopes, promises to provide decisive answers for the long-asked questions regarding the large-scale distribution in the local universe.

We are grateful to all our friends who have helped us collect these data over the years. This work was supported primarily by NSF grant AST 94-01519. Additional support for this work was provided by NASA through grant number GO-06579.02-95A from the Space Telescope Science Institute, which is operated by the Association of Universities for Research in Astronomy, Inc., under NASA contract NAS 5-26555.

APPENDIX A

THE FLOW MODEL

Our standard flow model consists of five components: Hubble flow, peculiar velocity, Virgo Attractor, Great Attractor, and quadrupole. Alternative models are possible as discussed above which center the quadrupole on Virgo or use different values of γ, but they give very nearly the same model velocity as a function of position. One caveat is that our measure of the mean flow velocities around the VA and GA are extremely uncertain for $r < 6$ Mpc for the VA and $r < 10$ Mpc for the GA.

We work in supergalactic coordinates, using a transformation from galactic to supergalactic coordinates by applying the rotation matrix

$$\begin{pmatrix} -\sin\phi_S & +\cos\phi_S & 0 \\ -\sin\theta_S\cos\phi_S & -\sin\theta_S\sin\phi_S & \cos\theta_S \\ +\cos\theta_S\cos\phi_S & +\cos\theta_S\sin\phi_S & \sin\theta_S \end{pmatrix} \tag{A1}$$

to galactic Cartesian coordinates, where $\phi_S = 47.^\circ37$ and $\theta_S = 6.^\circ32$.

Our value for the Sun's motion with respect to the CMB (hence transformation from heliocentric velocities to CMB reference frame) comes from Lineweaver et al. (1996), who find the Sun moving at 369 km s^{-1} toward SGL = 264.°31 and SGB = 48.°05.

Given a position (x, y, z) in supergalactic coordinates with respect to the Local Group, the first two terms of our model are

$$\boldsymbol{v} = H_0\boldsymbol{r} + \boldsymbol{w}\,, \tag{A2}$$

where $H_0 = 78.4$ and $\boldsymbol{w} = (-55, 143, -8)$.

The two attractors have a radial infall around them. Each causes a deviation from the above velocity of the form (eq. [4])

$$u_{\rm infall} = \tfrac{1}{3}H_0\, r_A\, \Omega_M^{0.6}\delta(r_A)[1+\delta(r_A)]^{-1/4}\,, \tag{A3}$$

where r_A is the distance from the point of interest to the attractor, $\Omega_M = 0.2$, and $\delta(r_A)$ is the overdensity in units of the background density at distance r_A from the attractor. The overdensity $\delta(r_A)$ is calculated from equation (7):

$$\delta(r_A) = \frac{\delta_0\, e^{-r_A/r_{\rm cut}}}{1-\gamma/3}\left(\frac{r_A}{r_c}\right)^{-3}\left[\left(1+\frac{r_A^3}{r_c^3}\right)^{1-\gamma/3} - 1\right]. \tag{A4}$$

δ_0 is evaluated by plugging in the distance from the LG to the attractor and matching to the model overdensities given below. The contribution to $\boldsymbol{v}$ is obtained as $u_{\rm infall}(\boldsymbol{r}_A - \boldsymbol{r})/|\boldsymbol{r}_A - \boldsymbol{r}|$.

The Virgo Attractor is found at $(-3.1, 16.6, -1.6)$ Mpc; it has overdensity $\delta_V = 0.974$; its infall exponent is $\gamma_V = 1.5$; the core radius is $r_c = 2$; and the cutoff radius is $r_{\rm cut} = 11.7$.

The Great Attractor is found at $(-36.7, 14.6, -17.1)$ Mpc; it has overdensity $\delta_G = 0.781$; its infall exponent is $\gamma_G = 2.0$; the core radius is $r_c = 2$; and the cutoff radius is $r_{\rm cut} = 49.5$.

Finally, the quadrupole contribution is found by multiplying $\boldsymbol{r}$ by the matrix

$$e^{-r2/2r_{\rm quad}^2}\begin{pmatrix} 2.57 & 2.04 & -7.87 \\ 2.04 & -11.12 & -3.63 \\ -7.87 & -3.63 & 8.55 \end{pmatrix}, \tag{A5}$$

where the quadrupole cutoff radius is $r_{\rm quad} = 50$ Mpc.

Our model for the (one dimensional) velocity dispersion as a function of position has four components added in quadrature. The first is an overall thermal velocity of 180 km s^{-1} (plus 50 km s^{-1} added in quadrature to account for typical redshift measurement error). The next two are components centered on the VA and GA at the positions listed above, with amplitudes 650 and 500 km s^{-1}, respectively, at the center, but falling off spatially as a Gaussian with a sigma of 2 Mpc. Finally, we incorporate a fourth component for the Fornax cluster, centered at $(-1.9, -15.0, -13.4)$ Mpc, with amplitude 235 km s^{-1} and again a spatial falloff with sigma of 2 Mpc.[4]

TABLE 1

ZERO POINTS FROM GALAXY GROUPS

Group	$\langle\overline{m}_I\rangle$	$(m-M)$	$\langle\overline{M}_I\rangle$
M31.....	22.74 ± 0.04	24.44 ± 0.10	−1.70 ± 0.11
N1023	28.26 ± 0.08	29.84 ± 0.08	−1.58 ± 0.11
Fornax.....	29.78 ± 0.03	31.41 ± 0.06	−1.63 ± 0.07
M81.....	26.27 ± 0.09	27.80 ± 0.08	−1.53 ± 0.12
Leo I.....	28.48 ± 0.04	30.08 ± 0.06	−1.60 ± 0.07
Virgo.....	29.41 ± 0.02	31.03 ± 0.06	−1.62 ± 0.06

[4] A FORTRAN program which implements this model can be found at http://www.ifa.hawaii.edu/~jt/SOFT/sbf2flow.f.

APPENDIX B

THE ZERO POINT

We find it difficult to choose a zero point for SBF using the various Cepheid distances that are available because we are faced with two options, each with virtues and faults. SBF is best measured in elliptical and S0 galaxies, and there are no direct Cepheid distance to such galaxies. Worse, there are presently no distances to spiral galaxies which appear to be tidally interacting with E or S0 galaxies (such as NGC 4647 and NGC 4649). We therefore are faced with the unpleasant choice of associating Cepheid distances to SBF galaxies via group associations, or else measuring SBF directly in spiral bulges where Cepheid distances exist.

B1. OPTION 1. CALIBRATING VIA GROUPS

For a group comparison we refer to Ferrarese et al. (1999) for Cepheid distances, but we reject the Coma groups because of the extreme confusion in that region, the Cen A group because it has a very large depth inferred from its angular extent across the sky, and the NGC 7331 group because it is really a galaxy-galaxy comparison with all the inherent worries described below. We also, for the sake of argument, do not agree with Ferrarese et al. in the inclusion of NGC 1425 as part of Fornax. It is statistically inconsistent with the other two Cepheid galaxies, NGC 1326A and NGC 1365; it is halfway between the Fornax and the Eridanus clusters, and its Cepheid distance is 0.40 mag more distant than the other two, very close to the 0.46 mag that we find for the mean distance between Fornax and Eridanus. We also concur with Ferrarese et al. in rejecting NGC 4639 from the Virgo cluster because it is 0.77 mag more distant. Finally, for M31, which is excluded from the SFD map, we follow Bianchi et al. (1996) and Ferrarese et al. (1999) in adopting the BH value of $E(B-V) = 0.08$, and then we use the SFD extinction ratios for consistency.

Table 1 lists the mean $\overline{m}_I$ we find for these groups, adjusted to a fiducial color of $(V-I)_0 = 1.15$, the distance modulus from Ferrarese et al., and the inferred SBF zero point, the absolute $\overline{M}_I$ at the fiducial color.

These groups paint a very consistent story: the zero point of the SBF calibration is $\overline{M}_I = -1.61 \pm 0.03$. The big advantage to using a group calibration is that we have many, very good SBF measurements in groups, as is reflected in the very small error bars.

The biggest disadvantage is that the association of spirals with ellipticals is shaky at best. As pointed out by Jacoby et al. (1992) the spirals in groups seem to lie outside of an elliptical core, as one might expect from the fragility of spirals and the harsh environment in the center of a group. However, in this case we are finding a sheet of five Cepheid bearing spirals at precisely the distance we assign to the core of the Virgo cluster, and two spirals at precisely the same distance as the core of Fornax. Had we included NGC 1425 as part of Fornax and NGC 4639 as part of Virgo, we might have expected the elliptical core to lie somewhere in between, leading to a brighter zero point by 0.1–0.2 mag.

B2. OPTION 2. CALIBRATING VIA GALAXIES

We again refer to Ferrarese et al. for Cepheid distances to galaxies where we have measured an SBF magnitude in the bulge. Table 2 lists the mean $\overline{m}_I$ we find for these six galaxies, adjusted to a fiducial color of $(V-I)_0 = 1.15$, the distance modulus from Ferrarese et al., and the inferred SBF zero point, the absolute $\overline{M}_I$ at the fiducial color.

These galaxies also are self-consistent: the zero point of the SBF calibration comes out as $\overline{M}_I = -1.80 \pm 0.08$. Given the wide range in the errors in the SBF measurement, it is also interesting to look at the median: $\overline{M}_I = -1.735$. Unfortunately, the galaxy average is inconsistent with the group calibration—they differ by 2.2 σ, which makes us very reluctant simply to take the group-galaxy comparison average.

The advantages of using the very same galaxies to carry out the calibration is that there is no doubt about the spatial relationship of the stars contributing to the SBF mean and the Cepheids. The disadvantage is that the SBF measurement is very hard, as is evidenced by the large error bars. We can only work on the side of the bulge which is in front of the plane of the disk; we must contend with dust in the bulge; we are affected by a portion of the disk which underlays the bulge we are analyzing; we encounter strong color gradients; and we always worry that somehow SBF might be different in spiral bulges than in ellipticals (despite the evidence to the contrary presented in SBF-I). We can try to improve our SBF measurements, but for some galaxies (e.g., NGC 4414) even *HST* resolution only reveals more and more dust threaded throughout the bulge. We do our best to make an accurate, unbiased measurement of SBF in spiral bulges, but we suspect that if there is a bias, it is probably in the sense of assigning too bright an SBF magnitude.

Given the probability that the ellipticals and spirals in these groups may be systematically separated in space, we feel that we must use the galaxy-galaxy calibration, although we are hedging our choice slightly by using the galaxy median. This is a situation which must be improved by further observation.

TABLE 2

ZERO POINTS FROM INDIVIDUAL SPIRALS

Galaxy	$\langle\overline{m}_I\rangle$	$(m-M)$	$\langle\overline{M}_I\rangle$
N0224.....	22.67 ± 0.06	24.44 ± 0.10	−1.77 ± 0.12
N3031.....	26.21 ± 0.25	27.80 ± 0.08	−1.59 ± 0.26
N3368.....	28.34 ± 0.21	30.20 ± 0.10	−1.86 ± 0.23
N4548.....	29.68 ± 0.54	31.04 ± 0.08	−1.36 ± 0.55
N4725.....	28.87 ± 0.34	30.57 ± 0.08	−1.70 ± 0.35
N7331.....	28.85 ± 0.16	30.89 ± 0.10	−2.04 ± 0.19

REFERENCES

Aaronson, M., et al. 1989, ApJ, 338, 654
Aaronson, M., Bothun, G. D., Mould, J., Huchra, J., Schommer, R., & Cornell, M. 1986, ApJ, 302, 536
Aaronson, M., Huchra, J., Mould, J., Schechter, P., & Tully, R. B. 1982a, ApJ, 258, 64
Aaronson, M., et al. 1982b, ApJS, 50, 241
Aaronson, M., Mould, J., Huchra, J., Sullivan, W., Schommer, R., & Bothun, G. D. 1980, ApJ, 239, 12
Ajhar, E. A., Lauer, T. R., Tonry, J. L., Blakeslee, J. P., Dressler, A., Holtzman, J. A., & Postman, M. 1997, AJ, 114, 626
Bianchi, L., Clayton, G. C., Bohlin, R. C., Hutchings, J. B., & Massey, P. 1996, ApJ, 471, 203
Blakeslee, J. P., Ajhar, E. A., & Tonry, J. L. 1999a, in Post-*Hipparcos* Cosmic Candles, ed. A. Heck & F. Caputo (Boston: Kluwer), 181
Blakeslee, J. P., Davis, M. Tonry, J. L., Dressler, A., & Ajhar, E. A. 1999b, ApJ, 527, L73
Blumenthal, G. R., Faber, S. M., Flores, R., & Primack, J. R. 1986, ApJ, 301, 27
Burstein, D., & Heiles, C. 1984, ApJS, 54, 33 (BH)
Cardelli, J. A., Clayton, G. C., & Mathis, J. S. 1989, ApJ, 345, 245
Colless, M., et al. 1999, in ASP Conf. Proc., Cosmic Flows Workshop, ed. S. Courteau, M. Strauss & J. Willick (San Francisco: ASP), in press
Courteau, S., Faber, S. M., Dressler, A., & Willick, J. A. 1993, ApJ, 412, L51
Courteau, S., & van den Bergh, S. 1999, AJ, 118, 337
Courteau, S., et al. 1999, in ASP Conf. Proc. Cosmic Flows Workshop, ed. S. Courteau, M. Strauss & J. Willick (San Francisco: ASP), in press
Dale, D., Giovanelli, R. Haynes, M., Campusano, L., Hardy, E., & Borgani, S. 1999, ApJ, 510, L11
Davis, M., Miller, A., & White, S. D. M. 1997, ApJ, 490, 63
Davis, M., Strauss, M. A., & Yahil, A. 1991, ApJ, 372, 394
de Vaucouleurs, G. 1958, AJ, 63, 253
de Vaucouleurs, G., de Vaucouleurs, A., Corwin, H. G., Jr., Buta, R. J., Paturel, G., & Fouqué, P. 1991, Third Reference Catalog of Bright Galaxies (New York: Springer) (RC3)
Djorgovski, S., & Davis, M. 1987, ApJ, 313, 59
Dressler, A., & Faber, S. M. 1990a, ApJ, 354, 13
———. 1990b, ApJ, 354, L45
Dressler, A., Faber, S. M., Burstein, D., Davies, R. L., Lynden-Bell, D., Terlevich, R. J., & Wegner, G. 1987, ApJ, 313, L37
Dressler, A., Tonry, J. L., Ajhar, E. A., Blakeslee, J. P., Lauer, T. R., Postman, M., & Holtzman, J. A. 2000, in preparation
Dubinski, J., & Carlberg, R. G. 1991, ApJ, 378, 496
Faber, S. M., & Burstein, D. 1988, in Proc. Vatican Study Week: Large-Scale Motions in the Universe, ed. V. C. Rubin & G. V. Coyne (Princeton: Princeton Univ. Press), 116
Faber, S. M., & Gallagher, J. S. 1979, ARA&A, 17, 135
Fadda, D., Girardi, M., Giuricin, G., Mardirossian, F., Mezzetti, M., & Biviano, A. 1996, ApJ, 473, 670
Ferrarese, L., et al. 1999, preprint (astro-ph/9908192)
Giavalisco, M., Macinelli, B., Mancinelli, P. J., & Yahil, A. 1993, ApJ, 411, 9
Gibbons, R. A., Fruchter, A. S., & Bothun, G. D. 1999, preprint (astro-ph/9903380)
Giovanelli, R., Haynes, M., Salzer, J., Wegner, G., da Costa, L., & Freudling, W. 1999, AJ, submitted (astro-ph/9807274)
Girardi, M., Fadda, D., Giuricin, G., Mardirossian, F., Mezzetti, M., & Biviano, A. 1996, ApJ, 457, 61
Han, M., & Mould, J. 1990, ApJ, 360, 448
Huchra, J., Geller, M., Clemens, C., Tokarz, S., & Michel, A. 1992, Bull. CDS, 41, 31
Hudson, M. J., Lucey, J. R., Smith, R. J., & Steel, J. 1997, MNRAS, 291, 488
Hudson, M. J., Smith, R. J., Lucey, J. R., Schlegel, D. G., & Davies, R. L. 1999, ApJ, 512, L79
Jacoby, G. H., et al. 1992, PASP, 104, 599
Kelson, D., et al. 2000, ApJ, submitted
Kennicutt, R., et al. 1998, ApJ, 498, 181
Lahav, O., Yamada, T., Scharf, C., & Kraan-Korteweg, R. C. 1993, MNRAS, 262, 711
Lauer, T. R., & Postman, M. 1994, ApJ, 425, 418
Lauer, T. R., Tonry, J. L., Postman, M., Ajhar, E. A., & Holtzman, J. A. 1998, ApJ, 499, 577
Lee, H., Hoffman, Y., & Ftaclas, C. 1986, ApJ, 304, L11
Lilje, P. B., Yahil, A., & Jones, B. J. T. 1986, ApJ, 307, 91
Lineweaver, C. H., Tenorio, L., Smoot, G. F., Keegstra, P., Banday, A. J., & Lubin, P. 1996, ApJ, 470, 38
Lu, N. Y., & Freudling, W. 1995, ApJ, 449, 527
Lynden-Bell, D., Faber, S. M., Burstein, D., Davies, R. L., Dressler, A., Terlevich, R. J., & Wegner, G. 1988, ApJ, 326, 19
Mathewson, D. S., Ford, V. L., & Buckhorn, M. 1992, ApJ, 389, L5
Navarro, J. F., Frenk, C. S., & White, S. D. M. 1996, ApJ, 462, 563
———. 1997, ApJ, 490, 493
Pahre, M. A., et al. 1999, ApJ, 515, 79
Peebles, P. J. E. 1976, ApJ, 205, 318
Riess, A. G., Press, W. H., & Kirshner, R. P. 1995, ApJ, 445, L91
Rubin, V. C. 1951, AJ, 56, 47
Rubin, V. C., Thonnard, N., Ford, K., Jr., & Roberts, M. S. 1976, AJ, 81, 719
Scaramella, R., Baiesi-Pillastrini, G., Chincarini, G., Vettolani, G., & Zamorani, G. 1989, Nature, 338, 562
Schechter, P. L. 1980, AJ, 85, 801
Schlegel, D. J., Finkbeiner, D. P., & Davis, M. 1998, ApJ, 500, 525 (SFD)
Shaya, E. J. 1984, ApJ, 280, 470
Shaya, E. J., Tully, R. B., & Pierce, M. J. 1992, ApJ, 391, 16
Silk, J. 1974, ApJ, 193, 525
Squires, G., Kaiser, N., Babul, A., Fahlman, G., Woods, D., Neumann, D. M., & Boehringer, H. 1996a, ApJ, 461, 572
Squires, G., Kaiser, N., Fahlman, G., Babul, A., & Woods, D. 1996b, ApJ, 469, 73
Strauss, M. A., Cen, R., & Ostriker, J. P. 1993, ApJ, 408, 389
Strauss, M. A., Yahil, A., Davis, M., Huchra, J. P., & Fisher, K. 1992, ApJ, 397, 395
Tammann, G. A., & Sandage, A. 1985, ApJ, 294, 81
Tonry, J. L. 1980, Ph.D. thesis, Harvard Univ.
Tonry, J. L., Blakeslee, J. P., Ajhar, E. A., & Dressler, A. 1997, ApJ, 475, 399 (SBF-I)
Tonry, J. L., & Davis, M. 1981, ApJ, 246, 680
Tonry, J. L., & Schneider, D. P. 1988, AJ, 96, 807
Tully, R. B. 1988, Nature, 334, 209
Tully, R. B., & Fisher, R. 1987, Nearby Galaxies Atlas (New York: Cambridge Univ. Press)
Willick, J. A. 1990, ApJ, 351, L5
———. 1999, ApJ, 522, 647
Willick, J. A., Strauss, M. A., Dekel, A., & Kolatt, T. 1997, ApJ, 486, 629
Worthey, G. 1994, ApJS, 95, 107
Yahil, A. 1985, in Workshop on the Virgo Cluster of Galaxies, ed. O. G. Richter & B. Binggeli (Munich: ESO), 350
Yahil, A. Sandage, A., & Tammann, G. A. 1980, in Les Houches Summer School, Session 32 (Amsterdam: North-Holland), 127
Yahil, A., Tammann, G. A., & Sandage, A. 1977, ApJ, 217, 903
Yamada, T., Tomita, A., Saito, M., Chamaraux, P., & Kazés, I. 1994, MNRAS, 270, 93